CrossMark

ORIGINAL PAPER

U–Pb zircon and biostratigraphic data of high-pressure/low-temperature metamorphic rocks of the Talea Ori: tracking the Paleotethys suture in central Crete, Greece

G. Zulauf[1] · W. Dörr[1] · J. Krahl[2] · Y. Lahaye[3] · V. Chatzaras[4,5] · P. Xypolias[6]

Abstract Inherited deformation microfabrics of detrital quartz grains and U–Pb (Laser ablation (LA)-ICPMS and ID TIMS) ages of detrital zircons separated from the Phyllite–Quartzite Unit s.l. of the Talea Ori, central Crete, suggest strikingly different source rocks. Albite gneiss of the lower Rogdia Beds includes Cambrian and Neoproterozoic rounded zircons with main U–Pb age peaks at 628 and 988 Ma. These and minor Paleoproterozoic and Archean peaks, together with the lack of Variscan-aged and Mesoproterozoic zircons, are similar to the age spectra obtained from the Phyllite–Quartzite Unit s.str. of the Peloponnesus and eastern Crete and from the Taurides. All of these zircons should be derived from the northeastern passive margin of Gondwana (Cimmeria). Metatuffites of the uppermost Rogdia Beds and metasandstone of Bali beach, on the other hand, include euhedral detrital zircons displaying a Variscan U–Pb age spectra at ca. 300 Ma

with concordia ages at 291 ± 3, 300 ± 1 Ma (Rogdia) and 286 ± 3, 300 ± 3, 313 ± 2 Ma (Bali). Both types of metasediments and their zircons are similar to those of the pre-Alpine basement and overlying Tyros Beds of eastern Crete, revealing a provenance at the southern active margin of Laurasia. Thus, in central Crete the Paleotethys suture should be situated inside the Rogdia Beds. Magmatic zircons separated from a rhyolite boulder of the lower Achlada Beds yielded a concordant U–Pb zircon age at 242 ± 2 Ma placing a maximum age for the deposition of the (meta) conglomerate from which the boulder was collected. This age is compatible with an Olenekian-early Anisian age of the underlying Vasilikon marble suggested by new findings of the foraminifera *Meandrospira* aff. *pusilla*. Both the Achlada Beds and the Vasilikon marble can be attributed to the lower Tyros Beds of eastern Crete. The Alpine deformation led to a pervasive mylonitic foliation, which is affecting most of the studied rocks. This foliation results from D2 top-to-the-north shearing, which post-dates the growth of blue amphiboles (crossite).

✉ G. Zulauf
g.zulauf@em.uni-frankfurt.de

1 Institut für Geowissenschaften, Universität Frankfurt a.M., Altenhöferallee 1, 60438 Frankfurt am Main, Germany

2 Agnesstraße 45, 80798 Munich, Germany

3 Geological Survey of Finland, P.O. Box 96, 02151 Espoo, Finland

4 Department of Geoscience, University of Wisconsin-Madison, Madison, WI 53706, USA

5 Department of Earth Sciences, Utrecht University, PO Box 80.021, 3508 TA Utrecht, The Netherlands

6 Department of Geology, University of Patras, 26500 Patras, Greece

Introduction

The reconstruction of pre-Neogene tectonic settings and paleogeography in the eastern Mediterranean is difficult because the pre-Neogene rocks have been stacked together during Oligocene/early Miocene subduction and collision of Apulia beneath the Pelagonian microcontinent following the closure of Neotethyan basins (e.g., Seidel et al. 1982; Dercourt et al. 1993; Xypolias and Doutsos 2000; Xypolias et al. 2007; Robertson 2006, 2012). This holds particularly
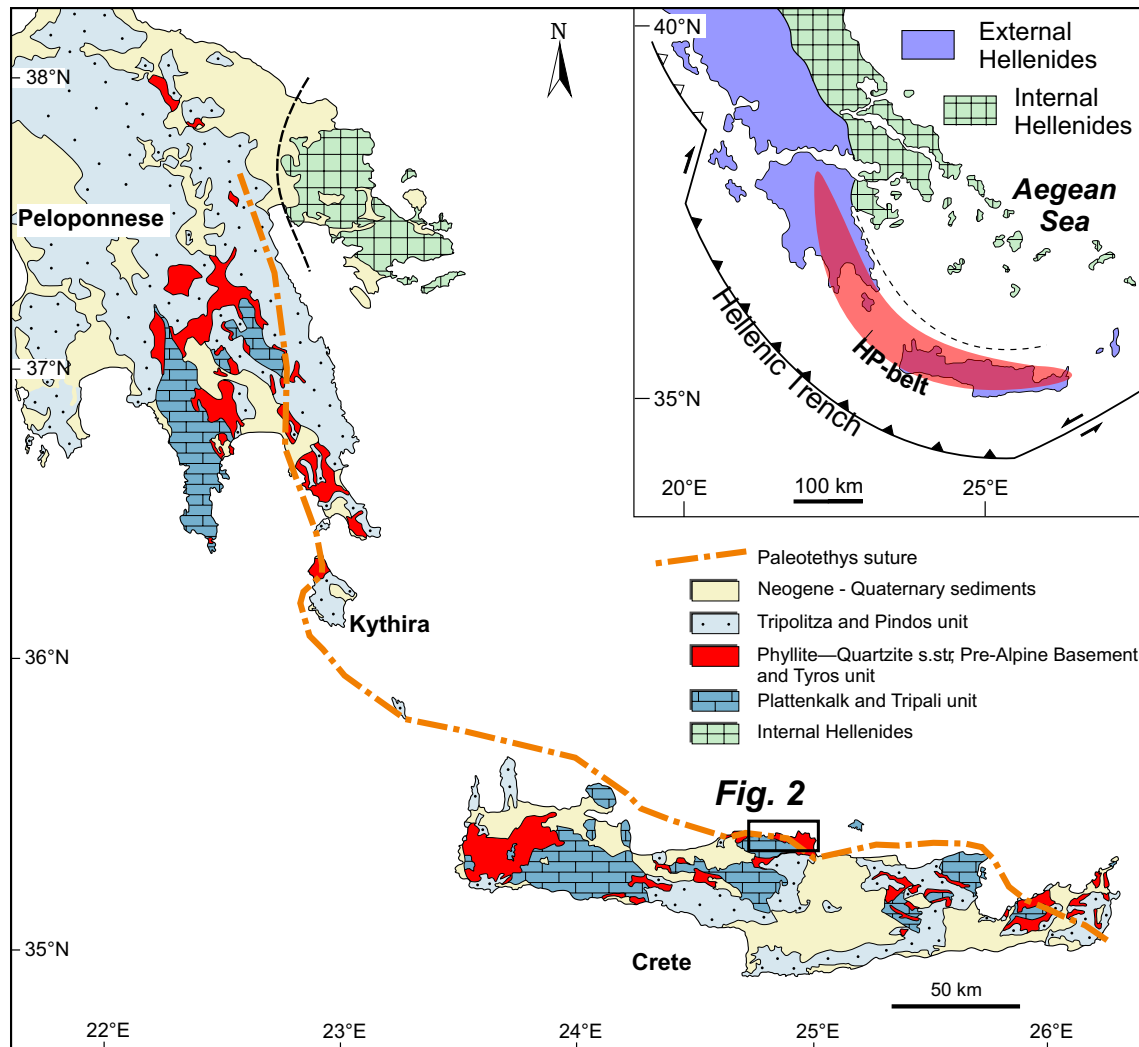
🖄 Springer

Fig. 1 Map showing distribution of main geotectonic units in the eastern Mediterranean region (modified after Xypolias et al. 2007). *Inset* shows the overall exposure of the high-pressure metamorphic rocks of the External Hellenides. *Black box* indicates outline of map shown in Fig. 2. The trace of the Paleotethys suture (*orange broken line*) is based on data published by Zulauf et al. (2014) and Chatzaras et al. (this volume, and this study)

for the External Hellenides exposed on Crete and the Peloponnesus (Fig. 1). Recent U–Pb studies of detrital zircons separated from rocks of eastern Crete revealed entire different pre-Alpine geodynamic settings for the Permo-Triassic Tyros (including the Variscan basement underneath) and the Phyllite–Quartzite Unit s.str. situated below the Variscan basement. Detrital zircons of the Phyllite–Quartzite Unit s.str. are restricted to Cambrian and older ages (Dörr et al. 2015; Chatzaras et al. this volume), whereas the detritus of the Tyros Unit and of parts of the Variscan basement include Variscan-aged zircons (Zulauf et al. 2014). For this reason, the tectonic contact between the Phyllite–Quartzite Unit s.str. and the Variscan basement/Tyros Unit has been interpreted as the suture of the Paleotethys that was closed in this domain during the Ladinian. During Ladinian collision, the

entire domain involved (sediments of the Phyllite–Quartzite Unit s.str., Variscan basement, and volcanosedimentary sequence of the Tyros Unit) underwent uplift and erosion. For this reason, Ladinian marine fauna has not been found in the Tyros Beds of Crete and the Peloponnesus, and parts of the Carnian sediments were deposited in a lacustrine environment (Zulauf et al. 2014, and references therein). In other domains, where the Variscan crystalline basement is lacking and the degree of Alpine high-pressure–low-temperature (HP–LT) metamorphism is higher than in eastern Crete, the position of the Paleotethys suture is not well constrained. This holds particularly for the Talea Ori domain of central Crete, where the rocks between the Plattenkalk (Talea Ori) and Tripolitza Unit are largely enigmatic concerning protolith age and structural evolution.
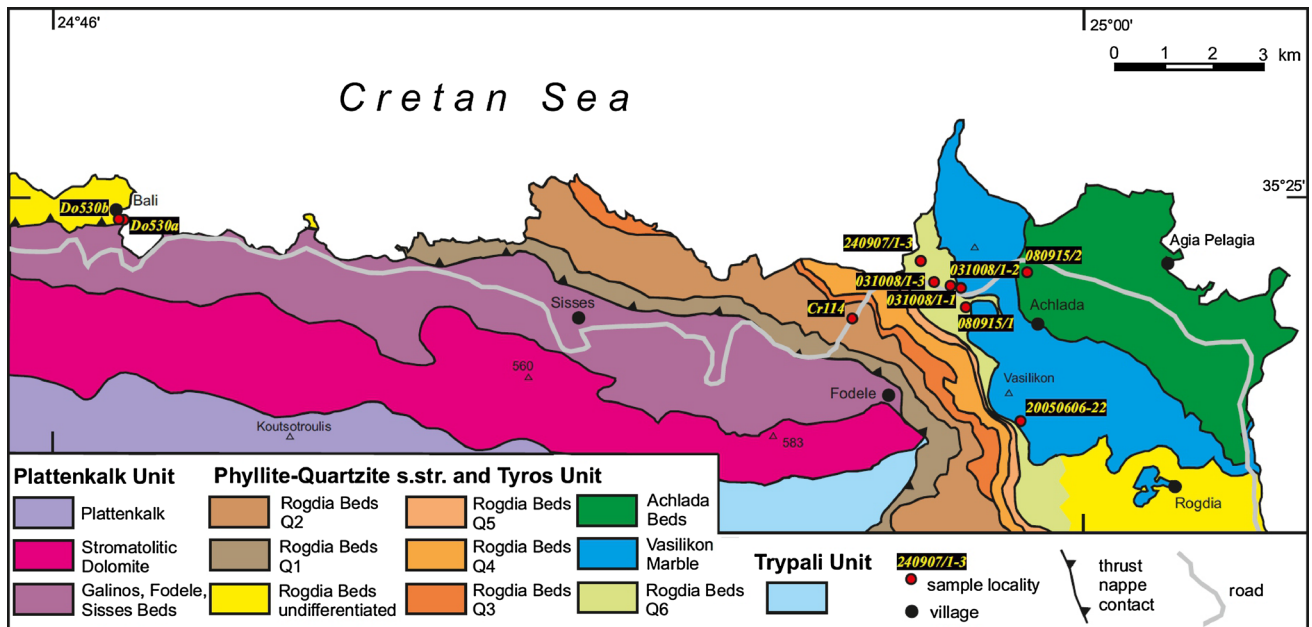
Fig. 2 Geological map of the Talea Ori compiled after Epting et al. (1972) and Richter and Kopp (1983). Sample localities are indicated

In the Talea Ori HP–LT metamorphic rocks of the Plattenkalk (Talea Ori) Unit and of the Phyllite–Quartzite Unit s.l. have been mapped (Fig. 2; Epting et al. 1972; Seidel et al. 1982; Hall and Audley-Charles 1983; Richter and Kopp 1983; Krahl et al. 1988; Kock et al. 2007). The protolith ages of the rocks of the Plattenkalk Unit are well constrained, whereas the age of the rocks of the Phyllite–Quartzite Unit s.l., subdivided into Rogdia Beds, Vasilikon marble, and Achlada Beds (Fig. 3), is largely unknown.

The present study focuses on these different units. We will present: (1) new U–Pb zircon ages separated from metasediments of the Rogdia and Achlada Beds to constrain the provenance and the maximum depositional age of these rocks, and (2) new findings of microfossils from the Vasilikon marble, which can be used to constrain the age of its protolith. The significance of the U–Pb ages and of the fossils will be discussed in the light of pre-Alpine stratigraphy and paleogeography. Concerning Tethyan nomenclature, we follow the concept of Robertson (2006): the term Paleotethys refers generally to older (i.e., pre-Mid-Jurassic) oceanic crust, while the term Neotethys is related to generally younger oceanic crust (i.e., Late Triassic–Early Cenozoic).

Regional geology

The rocks of the study area were affected by strong deformation and high-pressure/low-temperature metamorphism related to Alpine subduction/collision. For this reason, the structure of the rocks is complicated, fossils are rare and the age of many rocks is yet not known. Consequently, the geological maps published so far from this area differ significantly (Epting et al. 1972; Hall and Audley-Charles 1983; Richter and Kopp 1983; Kock et al. 2007; Katsiavrias et al. 2008).

The lowermost tectonostratigraphic unit of the study area is called *Talea Ori* or *Plattenkalk Unit*. Based on field mapping and fauna record (Epting et al. 1972; König and Kuss 1980; Krahl et al. 1988; Kock et al. 2007), the Plattenkalk Unit has been subdivided into (from stratigraphic bottom to top): Galinos Beds (Carboniferous to early–middle Permian); Fodele Beds (middle to late Permian); Sisses Beds (early Triassic to late Triassic); Stromatolithic Dolomite (late Triassic to Liassic); Plattenkalk s.str. (late Liassic and younger) (Fig. 3).

The Talea Ori Unit is tectonically overlain by the *Rogdia Beds* (Krahl et al. 1988), which largely consist of phyllite and quartzite. Layers of marble yielded Lower Triassic fauna at Skilármi (Epting et al. 1972) and south and west of Rogdia (Krahl et al. 1988). However, the marble at Skilármi could also be part of the lowermost Talea Ori (Plattenkalk) Unit (König and Kuss 1980; Richter and Kopp 1983). The eastern part of the Rogdia Beds has been subdivided into six different subunits (Q1–Q6; Richter and Kopp 1983; Fig. 2). Each subunit starts with a competent quartzite or metasandstone at the base (e.g., the Maskáli quartzite of Q1), whereas the higher parts are more phyllitic (Richter and Kopp 1983). The Q2 unit is characterized by a yellow metasandstone, which is less silicified and less cohesive
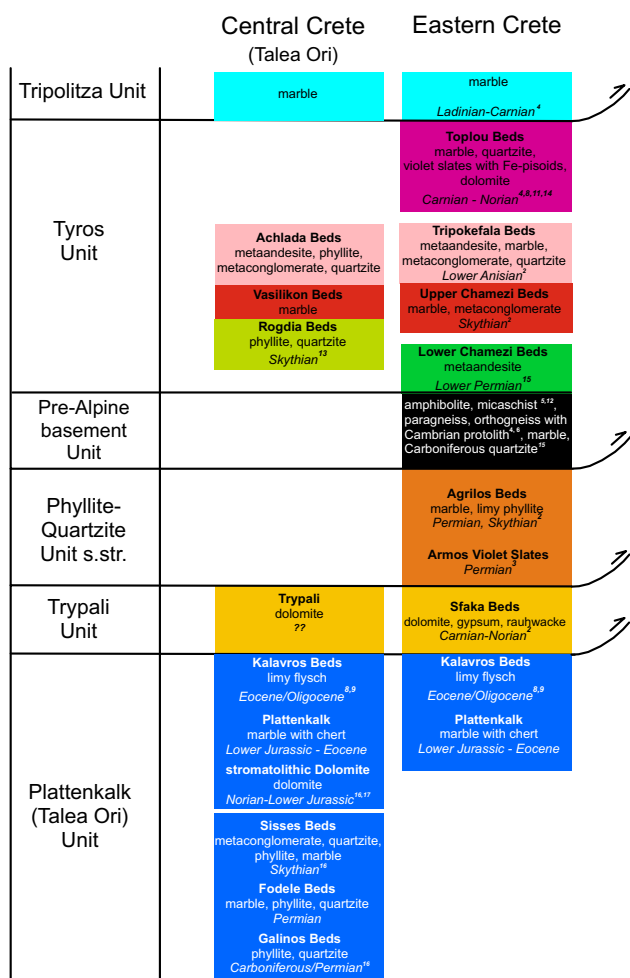
Fig. 3 Tectonostratigraphic sequence of Plattenkalk (Talea Ori), Trypali, Phyllite–Quartzite s.str., Pre-Alpine basement and Tyros Unit in central and eastern Crete. Key: 1 Krahl et al. (1983); 2 Krahl et al. (1986); 3 Kozur and Krahl (1987); 4 Haude (1989); 5 Franz (1992); 6 Romano et al. (2004, 2006); 7 Sannemann and Seidel (1976); 8 Fytrolakis (1972); 9 Bonneau (1973); 10 Cayeux (1902); 11 Fytrolakis (1967); 12 Seidel et al. (1982); 13 Krahl et al. (1988); 14 Zulauf et al. (2013); 15 Zulauf et al. (2014); 16 König and Kuss (1980); 17 Epting et al. (1972)

compared to the coarse-grained metaclastics of the other subunits. This metasandstone is fine- to medium-grained and shows thin layers of dark phyllite. The quartz grains of the metasandstone are embedded within a clayey matrix. The upper part of the Q6 subunit, situated just below the Vasilikon marble, shows thin layers of marble (Richter and Kopp 1983) and felsic layers, which are rich in feldspar and contain blue amphibole (crossite); these layers have been interpreted as metavolcanics (Seidel 1978). Other parts of the Rogdia Beds, exposed near Rogdia and near Bali, have yet not been ascribed to one of the above subunits and are thus depicted as undifferentiated Rogdia Beds in Fig. 2. The Bali rocks are particularly problematic. While the

gray metasandstone exposed at Bali beach is ascribed to the Rogdia Beds by Epting et al. (1972), Kock et al. (2007) have mapped the whole sequence of Bali as Galinos Beds, which are forming the lowermost member of the Plattenkalk (Talea Ori) Unit (see above).

The Rogdia Beds are overlain by the Vasilikon marble as defined by Epting et al. (1972) (Figs. 2, 3). It is a pale, massive marble, which shows fragments of greenschist at its base (Richter and Kopp 1983). On top of the Vasilikon marble, there is a sequence dominated by greenschists (metaandesites, Seidel 1978) referred to as *Achlada Beds*.

There are two major deformational phases recognizable in the Rogdia Beds (Hall and Audley-Charles 1983; Richter and Kopp 1983; Krahl et al. 1988). The earliest episode (D1) has produced a penetrative cleavage (S1) which is axial planar to tight to isoclinal mesoscopic folds with approximately N–S trending fold axes subparallel to a stretching/mineral lineation (Chatzaras et al. 2006). The second deformational episode (D2) is related to folding with an approximately E–W trending fold axes and axial surfaces dipping northwards. In thick slate sequences, the D2 episode has usually produced only a crenulation of the S1 cleavage, whereas in thick quartzites no folds are observed, and the D2 deformation has been accommodated by shearing and slip along lithologic boundaries (Hall and Audley-Charles 1983).

Analytical techniques

Lithology, faunal content and deformation microfabrics

The selected samples were investigated concerning the mineral composition, possible faunal content and the deformation microfabrics using thin sections. In order to reveal the sense of shear in cases of non-coaxial deformation, thin sections were produced from cuts oriented parallel to the mineral/stretching lineation and perpendicular to the dominant foliation.

U–Pb zircon analysis

Laser ablation (LA)-ICPMS method

Samples for isotope mass spectrometry were processed at the Institut für Geowissenschaften of Frankfurt University using standard mineral separation techniques. These include crushing and sieving, before concentration of heavy minerals by heavy liquids (bromoform, methyleniodide) and magnetic separation with a Frantz isodynamic separator. Handpicked zircon grains were mounted in 25-mm-diameter circular epoxy mounts and polished to expose a section at their inner core. Zircon U–Pb isotope analysis

was performed by Laser ablation (LA)-ICPMS technique using a Thermo-Finnigan Element II sector field ICPMS attached to a New Wave LUV213 laser ablation system ($\lambda = 213$ nm). Ablation was carried out in a He carrier gas in a low volume (2.5 cm^3) cell; laser beam parameters used were 30 µm diameter, 5 Hz repetition rate 75 % power output. Isotope data were acquired in peak-jumping mode on eight masses; 202, 204, 206, 207, 208, 232, 235 and 238. Background and ablation data for each analysis were collected over 90 s, with background measurements (carrier gas, no ablation) being taken over the first 30 s prior to initiation of ablation. Data were collected at time-resolved mode allowing acquisition of the signal as a function of time (ablation depth) and subsequently recognition of isotopic heterogeneities within the ablated volume. Raw data were processed offline using an Excel® spreadsheet program created by A. Gerdes. Mass discrimination of the MS and elemental fractionation during laser ablation were corrected by calibration against the GJ-1 zircon standard (Jackson et al. 2004), which was analyzed routinely during analytical sessions (three standard analysis at the beginning and end of every session of 33 unknowns, and two standard analyses every 10 unknowns). Prior to this correction, the change of elemental fractionation (e.g., Pb/U and Pb/Th ratios as function of ablation time and thus depth) was corrected for each set of isotope ratios by applying a linear regression through all measured ratios versus time, excluding some outliers (>2 s.e.), and taking the intercept $t = 0$ as the correct ratio. Changes in isotopic ratios arising from laser drilling into domains of distinct Pb/U ratio (core/rim), mineral inclusions and zones affected by Pb loss (metamictization/cracks), can usually be detected by careful monitoring of the time-resolved signal, such analyses are normally rejected. Common Pb correction was applied only when the interference- and background-corrected ^{204}Pb signal was significantly higher than the detection limit of about 20 cps. The latter is limited by the amount of Hg in the carrier gas and the accuracy to which the ^{202}Hg and thus the interfering ^{204}Hg can be monitored. Corrections made were based on common Pb composition given by the second stage growth curve of Stacey and Kramers (1975) for Neoproterozoic age (600 Ma). Data presentation was made with Isoplot (Ludwig 2001).

ID-TIMS-U–Pb zircon method

Zircon grains with the size of 100–200 µm were hand-picked from the >1.6 Amp fraction of the heavy mineral separates for the isotope dilution thermal ionization mass spectrometry (ID-TIMS). After washing with 6 N HCl and acetone, zircon grains were weighted, transferred to small Savillex beakers and put with 24 N HF for 6 h on the hotplate at 90 °C. The HF was decanted and the vials were loaded again with 24 N HF and a mixed ^{205}Pb/^{235}U spike. The small Savillex vials were then placed into a Parr bomb. After dissolution at 180 °C for 96 h and subsequent evaporation to dryness at ca. 80 °C on a hotplate, the sample was converted into chloride by adding 0.2 ml 3 N HCl. Chemical separation of Pb and U on 100 µl columns (ion exchange resin AG 1 × 8, 100–200 mesh). The U and Pb isotope ratios of zircon were obtained using a Finnigan MAT 261 mass spectrometer in static multicollector mode with simultaneous ion counting of ^{204}Pb. All isotopic ratios were corrected for mass fractionation (1.0 ± 0.3 ‰/a.m.u), blank (ca. 5 pg) and initial lead using the Stacey and Kramers (1975) model Pb composition. The Pb/U isotope ratios were plotted using Isoplot (Ludwig 2001), with error ellipses reflecting 2σ uncertainty. To verify the complete analytical procedure, standard zircons 91500, GJ 1 and M257 have been reproduced (see data of the Institut für Geowissenschaften of Frankfurt University in Nasdala et al. 2008). The U–Pb data are reported with 2σ uncertainties.

Results

Metasandstone at Bali

A dark gray sample of coarse-grained metasandstone (Fig. 4a) exposed at the beach of Bali (sample Do530a, E24°47′03″, N35°24′47″; Fig. 2) consists of mono- and polycrystalline detrital quartz grains, which are poorly sorted with grains up to 3 mm in diameter. In cases where the detrital grains are well preserved, it is obvious that these are angular to subangular. The quartz grains are very different concerning the deformation fabrics. Many of the quartz grains show evidence for high-temperature deformation, such as perpendicular sets of subgrains aligned parallel to the prism and basal planes (Fig. 5a), as well as orthogonal outlines of quartz grain boundaries. Some of the quartz grains are entirely recrystallized with new grains showing 120° triple points resulting in a foam structure. These fabrics should be inherited, as the Alpine deformation occurred at much lower temperatures, resulting in bulging of grain boundaries and relatively small new recrystallized grains. Other monocrystalline quartz grains show only prism-parallel subgrains or undulatory extinction. There are also many grains of white mica, which are up to 1 mm long. Less frequent are biotite and plagioclase. Both white mica and biotite show evidence for deformation, such as bending or kinking. Plagioclase shows inherited internal fabrics (S$_i$) portrayed by the shape-preferred orientation of opaque phases (Fig. 5b).

The zircons selected from sample Do530a yielded U–Pb ages between ca. 280 and ca. 2800 Ma (Supplementary Table 1, Fig. 6a). The maximum sedimentation age
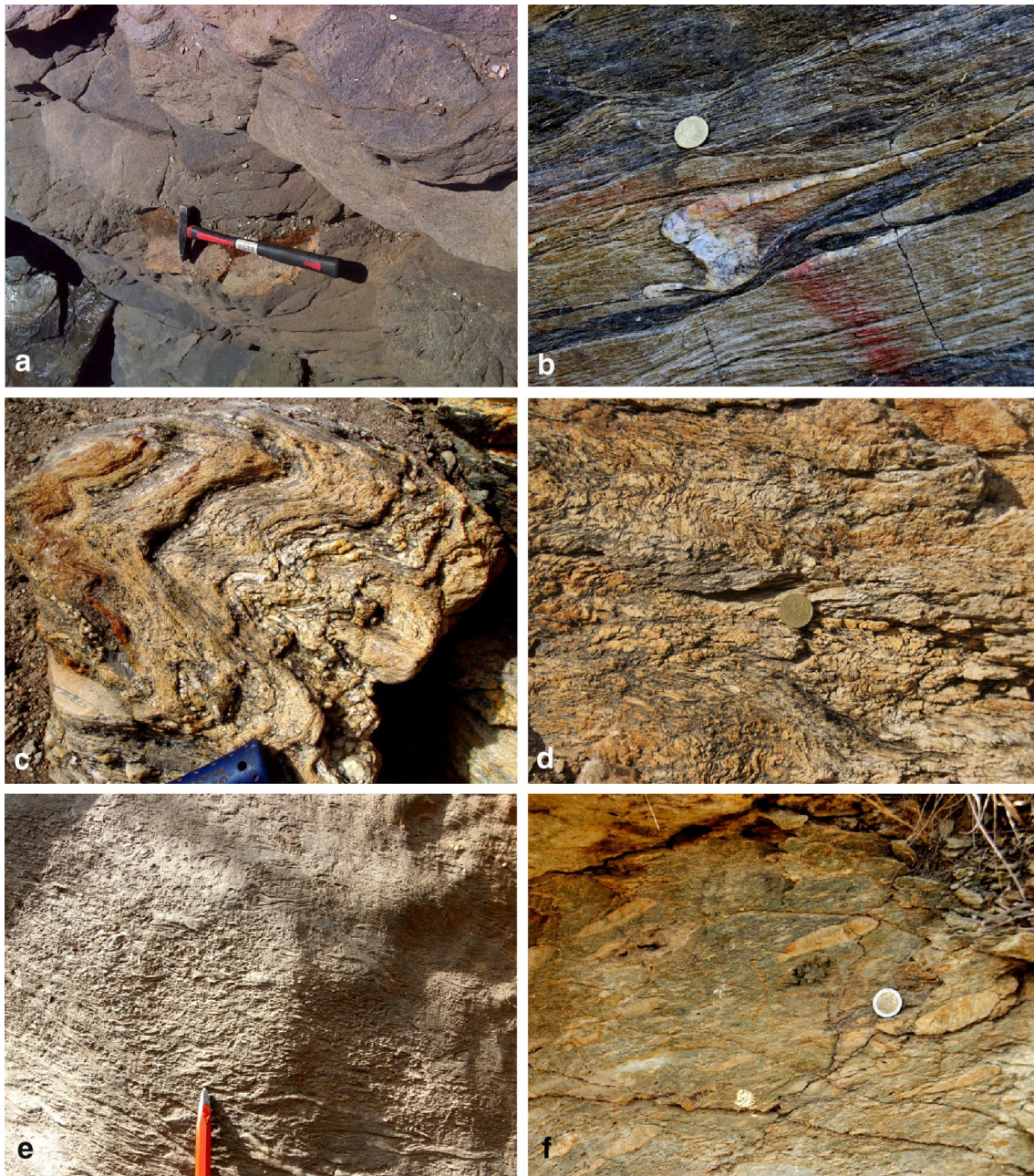
Fig. 4 Photographs of rocks investigated in the present study. **a** Dark metasandstone at Bali beach (sample Do530a). **b** *Pale brown* albite gneiss with thin layers of dark phyllite and sheared quartz vein of the lower Rogdia Beds (Q2 subunit); sample CR114. **c** Felsic quartzo-feldspathic rock (metatuffite) of uppermost Rogdia Beds (Q6 subu-nit); sample 240907/1-3. **d** (**c**) Felsic quartzo-feldspathic rock (metat-uffite) of uppermost Rogdia Beds (Q6 subunit); sample 090915-1. **e** Basal part of Vasilikon marble showing algae and other fossils (sample 090915-1). **f** Metaconglomerate of the basal Achlada beds (sample 080915/2)

has been constrained at 289 Ma, when considering the uncertainty of the youngest concordia age of four zircons (Fig. 7a). The sample contains 55 % Precambrian rounded detrital zircons with a small peak at ca. 800 Ma (Fig. 6c). Only 10 % of the zircons are older than 1 Ga. The Neo-proterozoic age group (45 %) is split into three parts (10 % Ediacaran, 17 % Cryogenian, and 18 % Tonian zircons).

The main group of the Paleozoic detrital zircons (39 %) is Late Carboniferous in age. The most significant age peak is present at ca. 310 Ma (Fig. 6e). Apart from the concordia age at 286 ± 3 Ma, there are concordia ages at 300 ± 3 and 313 ± 2 Ma (Fig. 7a–c). These late Variscan-aged zircons are largely euhedral (Fig. 8). The same holds for Silurian zircons, which, however, are less significant, with only two
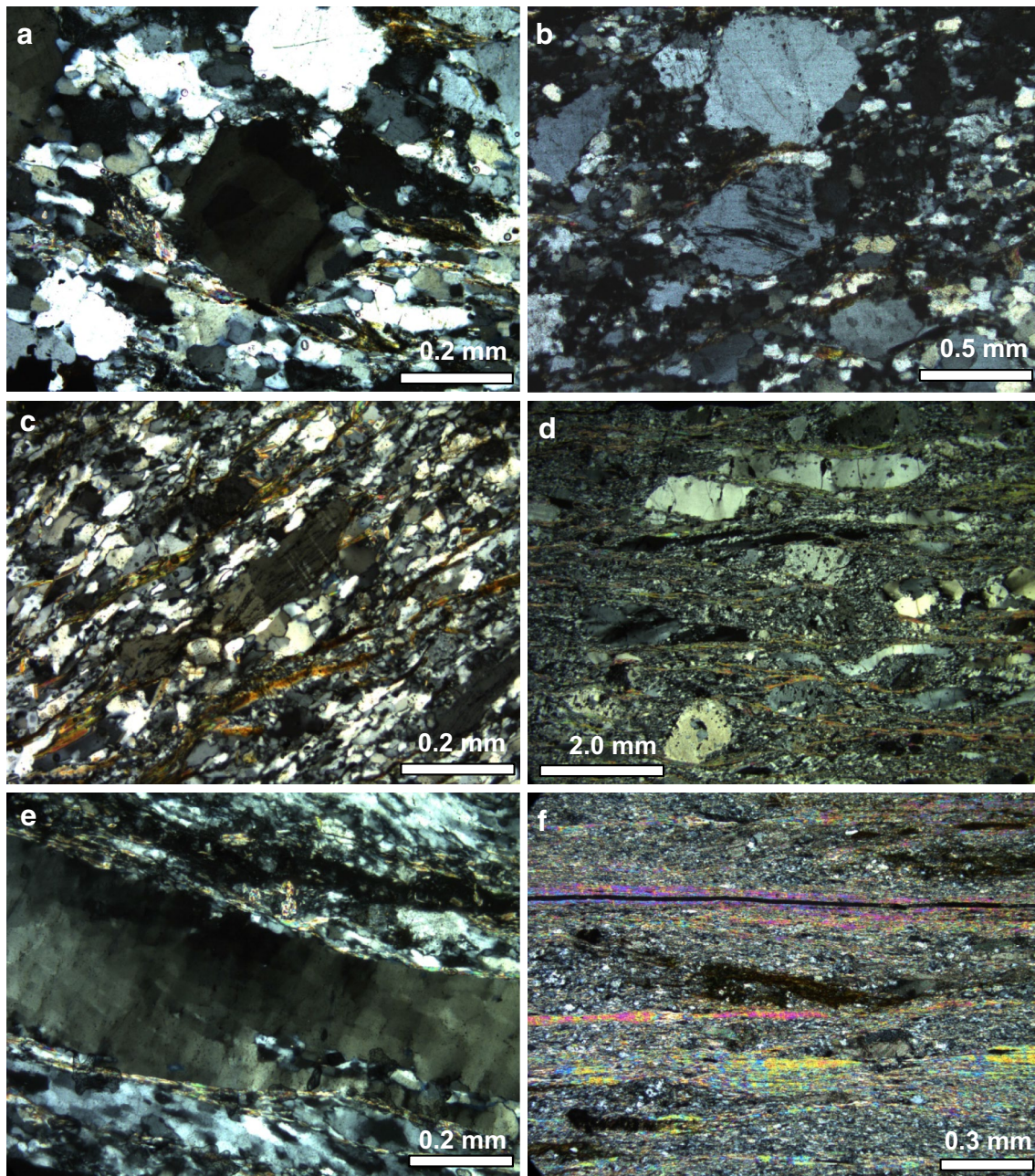
Fig. 5 Mircrophotographs of investigated rocks taken with crossed polarizers. **a** Chessboard-type subgrains in detrital quartz grain of Bali metasandstone indicates high-temperature deformation in the source domain; sample Do530a; **b** Detrital plagioclase in Bali metasandstone showing an inherited internal fabric (S_i), which results from the shape-preferred orientation of opaque phases. **c** Albite clast with internal fabric (S_i) and deformation twins embedded in recrystallized foliated matrix consisting of quartz, albite and phyllosilicates; Rogdia Beds (Q2 subunit); sample Cr114. **d** Porphyroclasts of quartz and albite in fine-grained largely recrystallized matrix of quartz and feldspar as well as aligned phyllosilicates; asymmetric pressure shadows behind these prophyroclasts indicate top-to-the-north sense of shear (*dextral* in the photograph); felsic gneiss layer in uppermost Rogdia Beds (Q6 subunit); sample 031008/1-1. **e** Close-up view of (**d**) showing large quartz clast with chessboard-type subgrains. **f** Phyllite of the Q6 subunit of the Rogdia Beds with *dark parts* consisting of biotite and chlorite; sample 031008/1-3

zircons compared to the Varisan-aged zircons (Fig. 6c). Similar low amounts are present in the Cambrian, Ediacaran, Cryogenian, Tonian and Stenian (Fig. 6c). Even less important are Paleoproterozoic and Archean ages (Fig. 6a).

It is important to note that most of the zircons older than Silurian are rounded or subangular (Fig. 8).

A second fine-grained sample of metasandstone (Do530b) has been collected from a road cut in Bali village
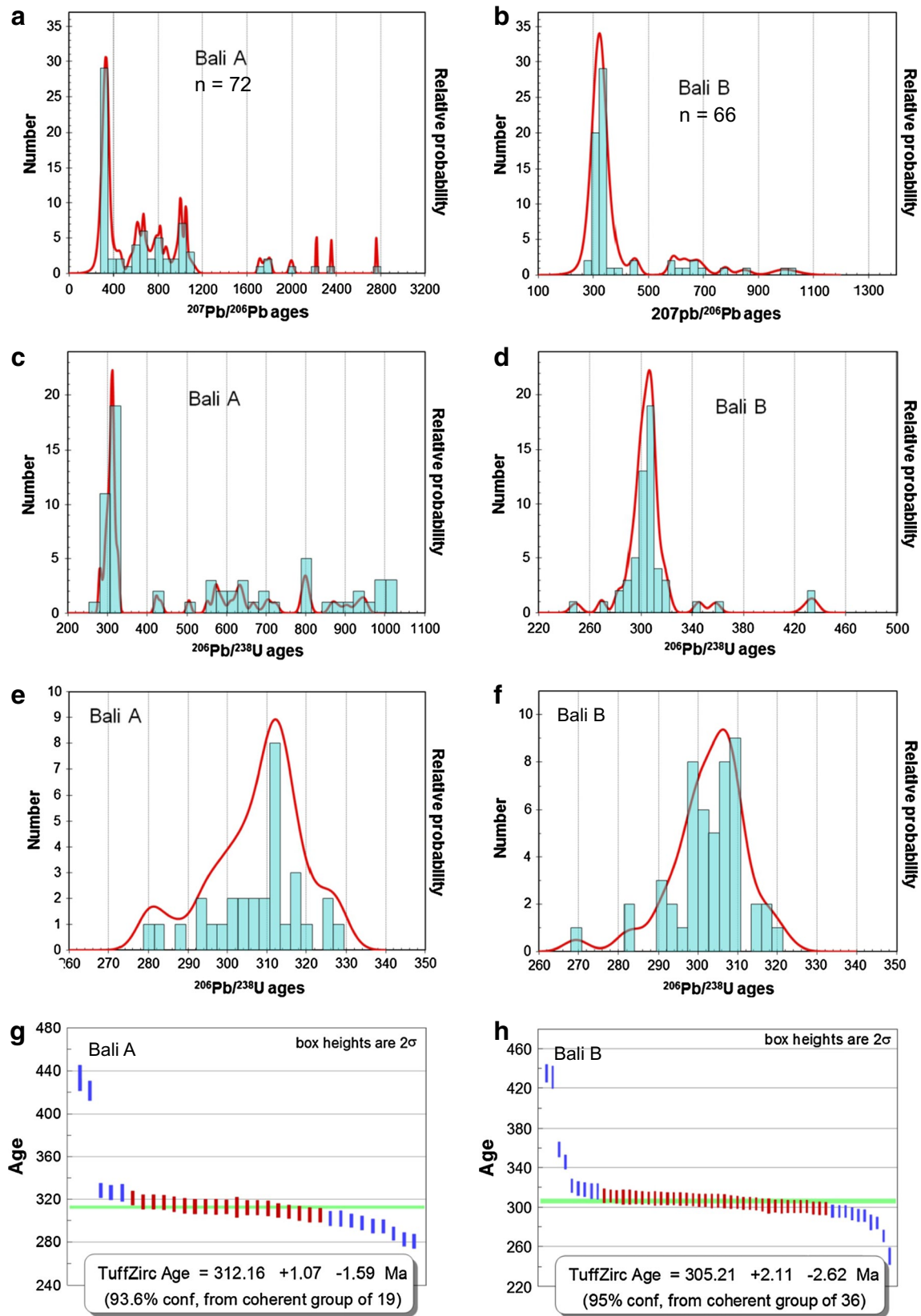
Fig. 6 Density plots of detrital zircons separated from coarse-grained (**a**, **c**, **e**, **g**) and fine-grained (**b**, **d**, **f**, **h**) sandstone of Bali. Bali A = coarse-grained metasandstone (sample Do 530a); Bali B = fine-grained metasandstone (sample Do 530b)
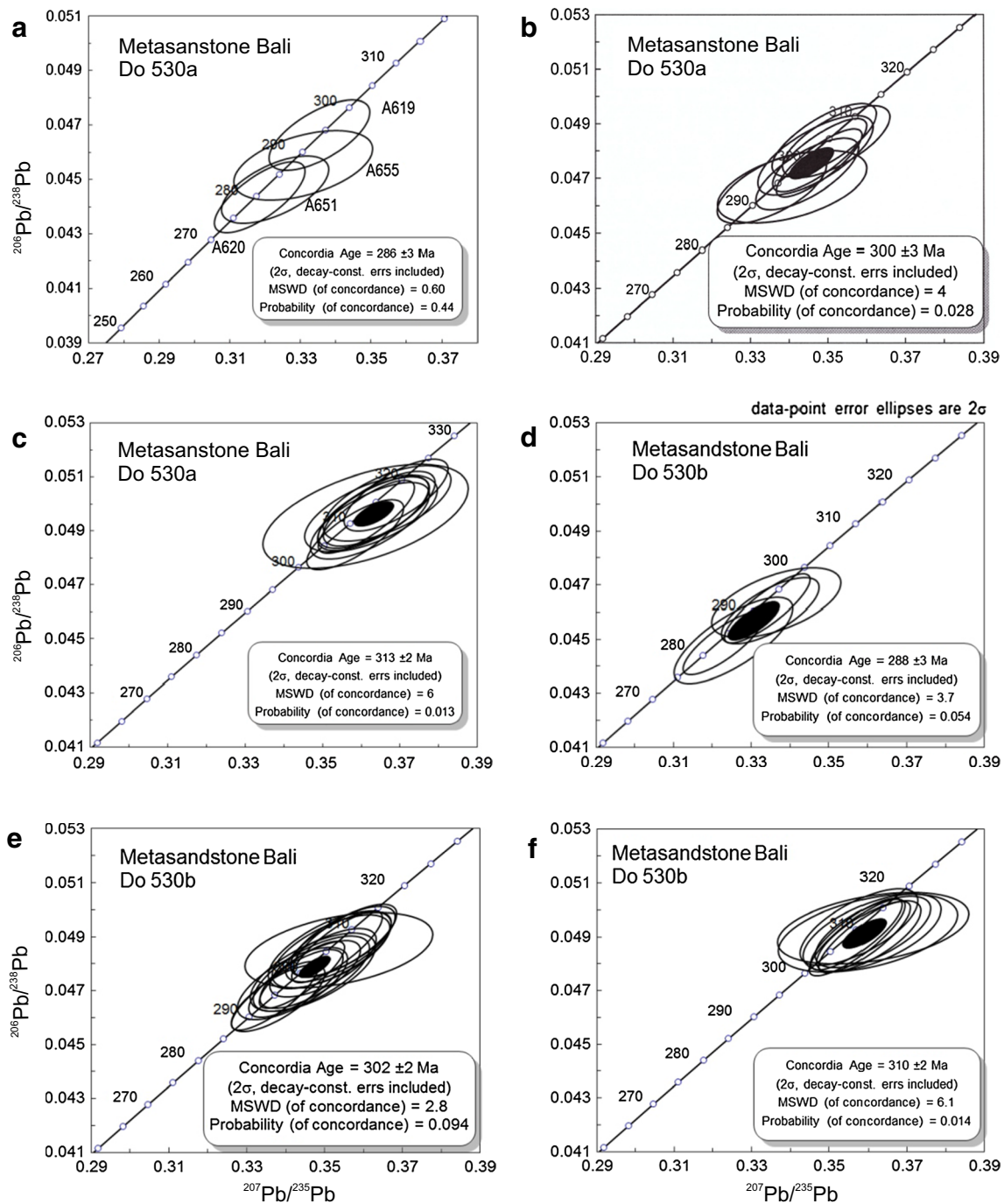
Fig. 7 U–Pb concordia plots of coarse- and fine-grained Bali metasandstone (samples Do 530a, and Do 530b, respectively)

(E24°46′58″, N35°24′44″, Fig. 2). This sample is very similar to the coarse-grained sample Do530a concerning the poor sorting and the different types of quartz grains. The amount of phyllosilicates (white mica and biotite), however, is higher.

The distribution of detrital zircon ages is also similar to that of sample Do530a (Supplementary Table 2). The maximum sedimentation age has been constrained at 291 Ma,

when considering the uncertainty of the youngest concordant zircon (Fig. 7d). This age fits well with that of sample Do530a. The sample Do530b contains only 17 % Precambrian rounded detrital zircons without any prominent peak. Zircons older than Stenian are lacking. In contrast to sample Do530a (39 %), the Late Carboniferous age group of sample Do530b is with 67 % much higher, but the most significant age peaks are similar (Fig. 6f). Apart from the
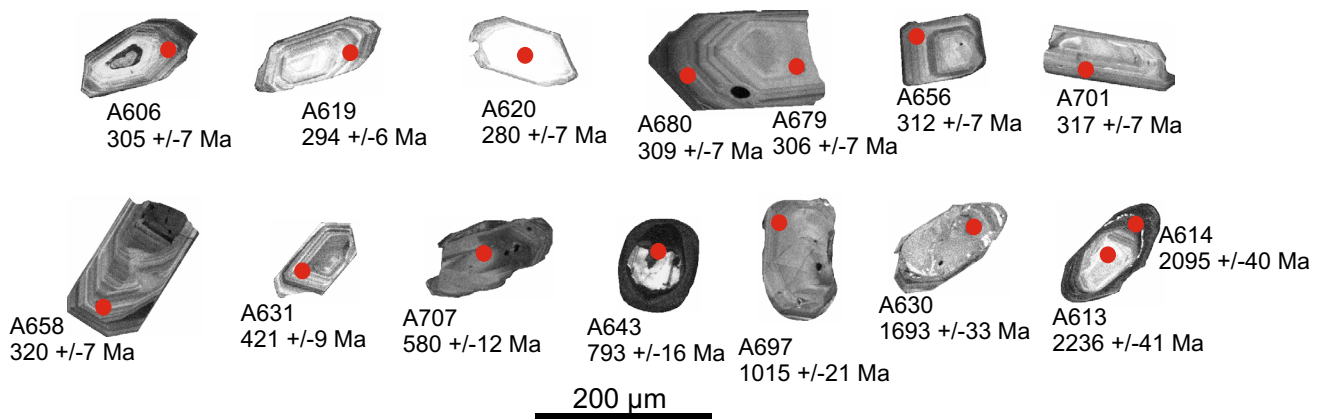
Fig. 8 Representative cathodoluminescence (CL) images of analyzed zircons separated from the coarse-grained metasandstone of Bali beach (sample Do 530a)

concordia age at 288 ± 3 Ma, the main peaks are defined by concordia ages at 302 ± 2 and 310 ± 2 Ma (Fig. 7e, f). Few zircons are present in the Silurian and in the Proterozoic. The Proterozoic age spectrum is similar to that of sample Do530a (Fig. 6b).

Albite gneiss of lower Rogdia Beds (Q2 subunit)

The albite gneiss is exposed along the highway between Sisses and Iraklion, ca. 2 km north-northeast of Fodele (sample Cr114; E24°56′57″, N35°23′40″, Fig. 2). This sample should be part of the Q2 subunit (yellow metasandstone) mapped by Richter and Kopp (1983). The analyzed albite gneiss is pale brown and includes thin layers of dark phyllite. Vein quartz is folded and sheared (Fig. 4b). The albite gneiss consists of quartz, albite and less amounts of white mica and biotite. The dominant foliation results from stretched quartz and aligned white mica. Tourmaline is

present as accessory mineral. Quartz is entirely recrystallized. Albite is present as a newly grown phase with a diameter up to 1 mm (Fig. 5c). The orientation of an internal foliation of albite (S_i) is different to the external foliation (Se), which is the dominant foliation of the gneiss. Albite shows deformation twins and pressure shadows, the latter consisting of white mica. Whereas white mica is largely aligned parallel to the dominant foliation, biotite is frequently oblique to this foliation. Non-coaxial deformation is indicated by asymmetric pressure shadows behind albite and oblique orientation of the albite blasts with respect to the dominant foliation.

The age spectrum of detrital zircons is strikingly different to that reported from the Bali metasandstones (Supplementary Table 3). Variscan-aged zircons are entirely lacking. Paleozoic (Cambrian) zircons are present at only 4 % (Fig. 9a, b). There are 72 % Neoproterozoic, 16 % Paleoproterozoic and 8 % Archean zircons (Fig. 9a). The amount
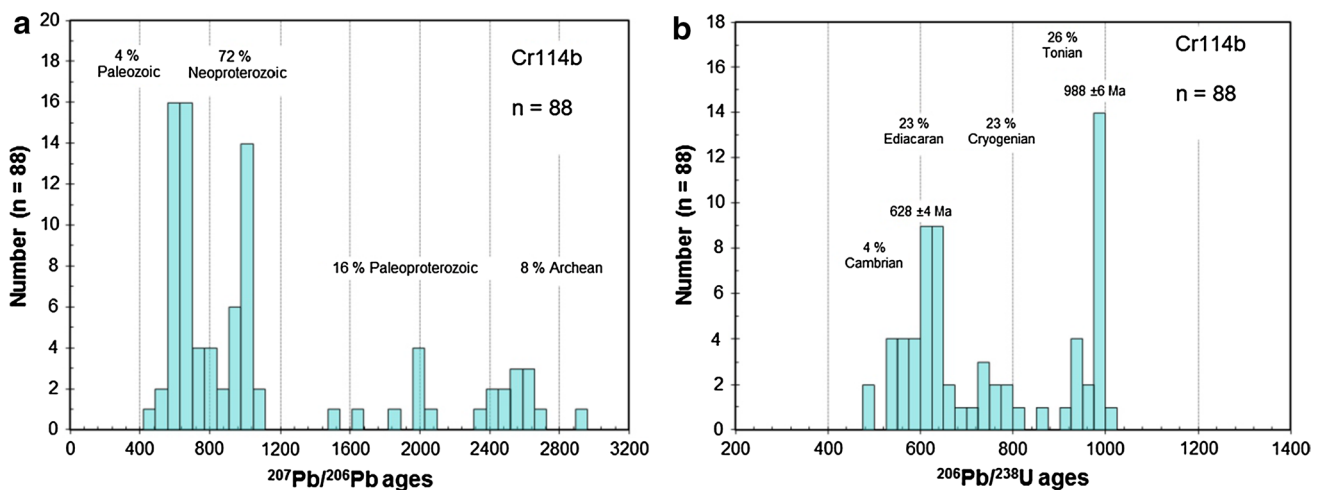

Fig. 9 Density plots of detrital zircons separated from albite gneiss of the lower Rogdia Beds (Q2 subunit); sample Cr114
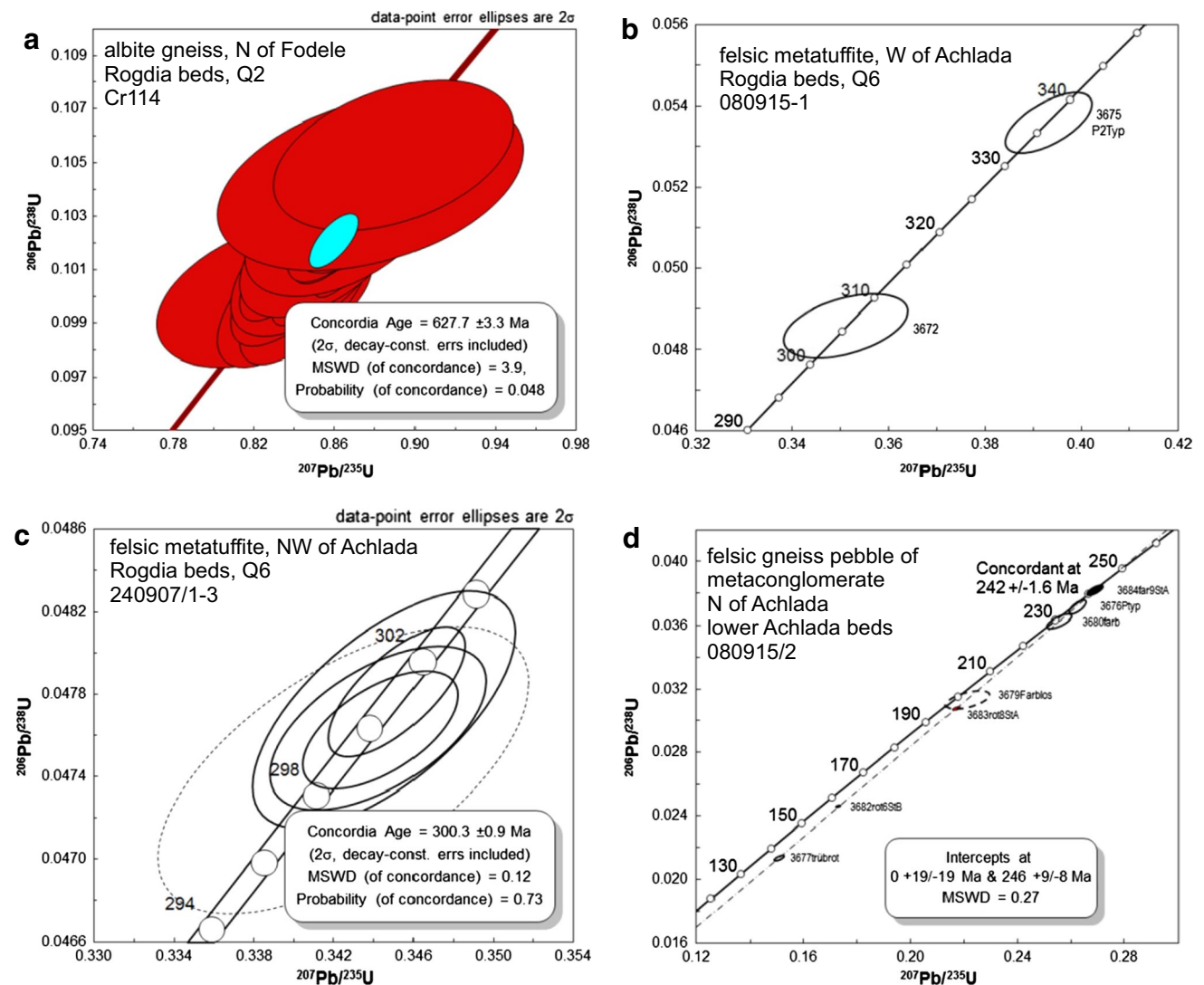
Fig. 10 U–Pb concordia plots of detrital zircons separated from different units of the Rogdia and Achlada Beds

of Ediacaran (23 %), Cryogenian (23 %) and Tonian (26 %) zircons is almost the same (Fig. 9b). The most striking peak is present in the Tonian at 988 ± 6 Ma. A further peak is present in the Ediacaran with a concordia age at 627.7 ± 3.3 Ma (Fig. 10a). Further, but smaller peaks are present at ca. 2.0 and 2.5 Ga (Fig. 9a). Most of the analyzed zircons are rounded to subangular (Fig. 11).

Meta-volcanosedimentary sequence of uppermost Rogdia Beds (Q6 subunit)

The uppermost part of the Rogdia Beds, mapped as Q6 subunit by Richter and Kopp (1983), are characterized by different types of phyllite and quartzite. A striking feature of the Q6 subunit is felsic layers, which are rich in quartz and feldspar (Fig. 4c, d). Seidel (1978) analyzed blue amphibole (crossite) inside these felsic layers and interpreted the latter as felsic tuffs.

Oriented samples of the Q6 subunit were collected for microfabric analyses along the highway Sisses-Heraklion. *Sample 031008/1-1* (N35°23′55.2″ E24°58′21.5″) is a mylonitic felsic gneiss, which is present in the uppermost parts of the Q6 subunit just below the Vasilikon marble. It consists of quartz, plagioclase, white mica, and K-feldspar (Fig. 5d). Quartz is present in the matrix of the rock in form of recrystallized grains, but also occurs as relatively large monocrystalline lenses or ribbons, up to 1 cm in length, some of which displaying a striking chessboard pattern because of perpendicular sets of prism- and basal-parallel subgrains (Fig. 5e). These large grains show a shape-preferred orientation, which contributes to the mylonitic foliation. There are many plagioclases up to 1 mm in diameter.
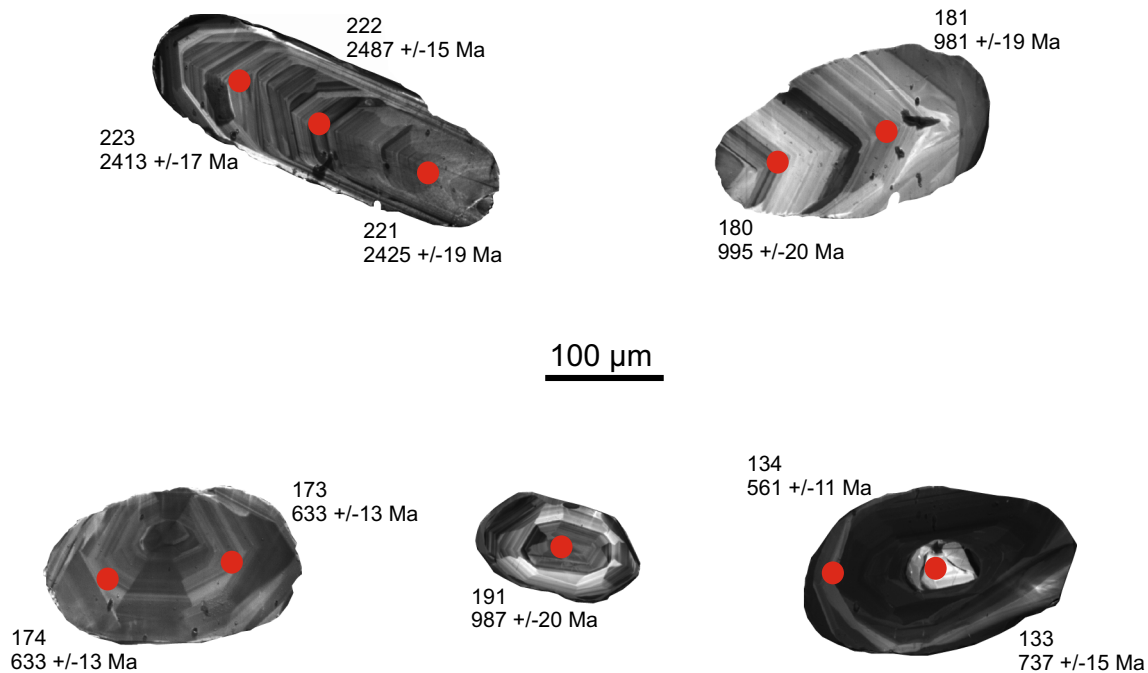
Fig. 11 Representative cathodoluminescence (CL) images of analyzed zircons separated from the albite gneiss of the lower Rogdia Beds (Q2 subunit); sample Cr114

Their asymmetric arrangement in sections cut perpendicular to the mylonitic foliation and parallel to the stretching lineation (*XZ*-sections) suggests non-coaxial deformation and top-to-the-north sense of shear (Fig. 5d). The latter is also indicated by asymmetric pressure shadows of quartz behind rigid plagioclase and by SC fabrics. In many cases, the central part of the plagioclase is largely altered by the growth of numerous tiny new minerals such as sericite, zoisite, and epidote, whereas the margin of the crystal is clear and free from inclusions. White mica is oriented parallel to the main foliation.

A further oriented *sample 031008/1-3* is a phyllite, which in hand specimens shows striking dark spots, the latter up to 4 mm in diameter. The clear matrix of this rock is phyllitic and consists of quartz, white mica, biotite and calcite. Calcite of the pale matrix is also present in form of lenses. Larger calcite crystals display type II deformation twins (sensu Burkhard 1993). The dark spots consist of biotite and chlorite. Similar to the phyllosilicates of the pale matrix, the dark spots show a shape-preferred orientation with the long axes aligned subparallel to the main foliation (Fig. 5f) and the N–S trending stretching lineation. The striking compositional contrast between the phyllitic matrix and the mafic spots suggests metatuffite.

Two samples of the felsic layers in the Rogdia beds have been selected for microfabric analysis and for U–Pb dating of zircons. One of these *samples (080915/1)* has been collected 1.5 km west of Achlada along the old road

Achlada–Fodele (E24°58′31″, N35°23′52″, Fig. 2). This mica-bearing quartzite is well foliated because of a compositional layering defined by quartz and mica-rich domains, and a shape-preferred orientation of white mica. The foliation is affected by folding, with the fold-axial planes being subhorizontal (Fig. 4d). Apart from quartz and white mica, there are few euhedral pyrite grains, which show pressure shadows of fibrous quartz. Quartz veins oriented subperpendicular to the main foliation have been sheared during late deformation increments. Another sample located few meters east of sample 080915/1 also consists largely of quartz and white mica, but shows few grains of plagioclase. Plagioclase is present inside the quartz matrix, but also occurs more frequent as larger grains in specific layers oriented parallel to the main foliation. U–Pb (TIMS) dating of the only two euhedral detrital zircons of the sample 080915/1 yielded concordant ages at 306 ± 4 and 337 ± 4 Ma (Fig. 10b; Supplementary Table 5).

A second *sample (240907/1-3)* collected also for dating is located southwest of the hill Bobias Vounou (N35°24′19.9″, E24°57′46.9″, Fig. 2). This rock shows a tight mylonitic foliation defined by stretched quartz and feldspar and a shape-preferred orientation of phyllosilicates. The stretching lineation on the mylonitic planes is N–S directed. The mylonitic foliation was folded around E–W trending axes (Fig. 4c), which led to a widely spaced crenulation cleavage. The rock consists of albite (>50 % according to XRD analysis), quartz, white mica, biotite and
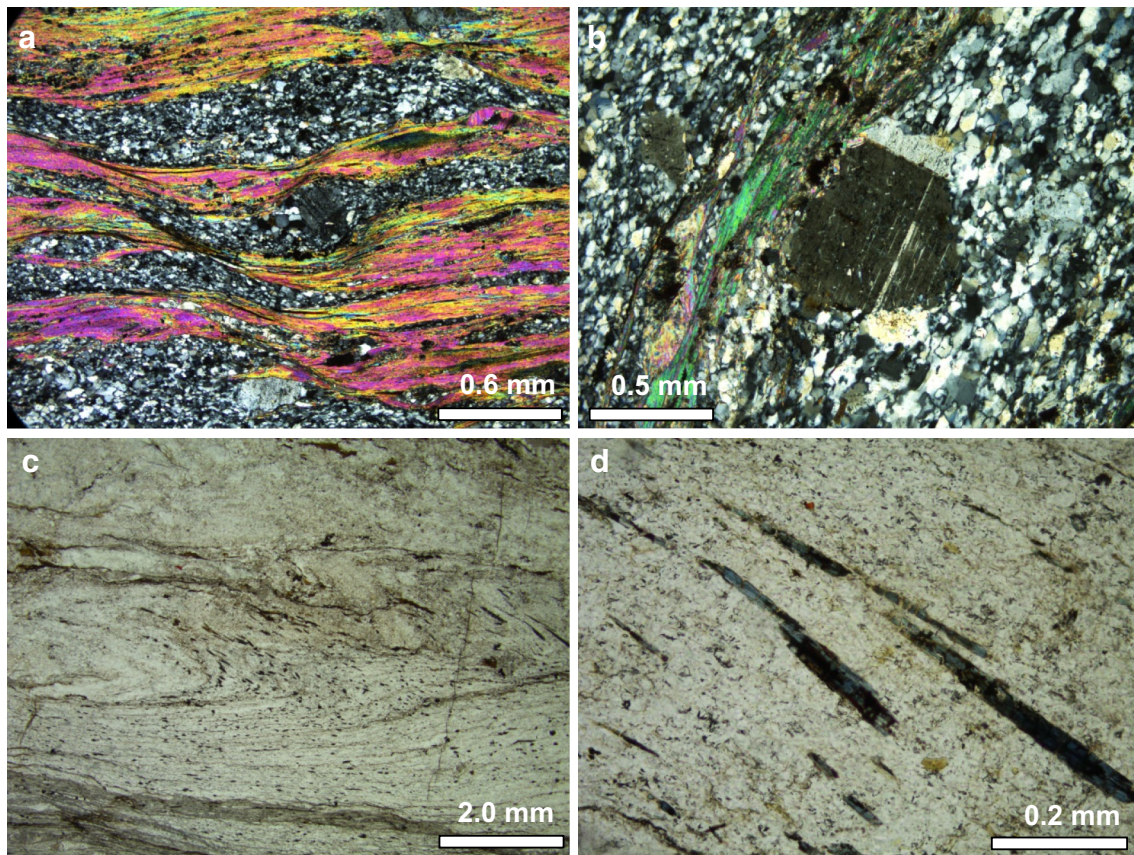
Fig. 12 Microphotographs of dated felsic layer of the Rogdia Beds (Q6 subunit); sample 24-09-07/1-3. **a** The main foliation (S2), defined by alternations of quartzo-feldspathic and phyllosilicate-rich layers, is affected by shear bands, which indicate a top-to-the-north sense of shear; crossed polarizers. **b** Albite clast in fine-grained mylonitic matrix is optically zoned and shows two sets of twins (after albite and pericline law) as well as marginal recrystallization by bulg- ing of grain boundary, crossed polarizers. **c** Isoclinal intrafolial fold post-dates the growth of blue amphibole (crossite, dark lath-shaped phases); the main foliation (S2) is horizontal in the photograph; paral- lel polarizers. **d** Close-up view of (**c**) showing aligned *blue* crossite inside the quartzo-feldspathic mylonitic matrix; *dark parts* inside the crossite reflect previous mafic mineral, most of which has been replaced by crossite; parallel polarizers

blue amphibole, which should be crossite (Seidel 1978). Accessory minerals are epidote and opaque phases. Quartz is pervasively recrystallized. Plagioclase is present in form of both relics of large grains (up to 2 mm in size) and as recrystallized grains. The former large grains show defor- mation twins, which in few cases are present as two sets, one according to the albite and the other according to the pericline law (Fig. 12b). Lath-shaped crossite is up to 1 mm long and shows a grain-shape fabric (Fig. 12d). Most of the blue amphiboles include relics of dark minerals, which might be previous amphibole or other mafic phases that were replaced by the blue amphibole during Alpine HP–LT metamorphism. Crossite is restricted to certain quartz- and feldspar-rich layers, which are isoclinally folded (Fig. 12c). These early isoclinal folds are present only as relics, and the folded foliation (S1) reflects the first deformation event (D1), which led to the grain-shape fabric of crossite. The D1-folds are forming intrafolial folds with respect to the dominant mylonitic foliation (S2), which results from

pervasive D2 top-to-the-north shearing as is indicated by shear-band fabrics and by asymmetric pressure shadows of quartz behind large feldspar (Fig. 12a). Crossite is also affected by boudinage, which might be related either to D1 or to D2 shearing. Folding of the main foliation, S2, around E–W trending axes should be related to a third deformation event (D3).

The detrital zircons of sample 240907/1-3 have been dated using both ID-TIMS and Laser-ICPMS (Supplemen- tary Tables 4, 5). The sample contains only 24 % Precam- brian rounded detrital zircons without any prominent peak. Only 5 % of the zircons are older than 1 Ga. The main group of the Paleozoic detrital zircons (57 %) is Late Car- boniferous in age. The most significant U–Pb age peaks are present at 280 ± 4, 291 ± 3 and ca. 301 ± 1 Ma (Fig. 13a– c, mean ages). They are similar to the samples described above. A third, but less prominent peak is present at ca. 580 Ma (Ediacaran). Further small peaks occur in the Cryo- genian (ca. 700 Ma), Tonian (ca. 850 and 930 Ma), Siderian
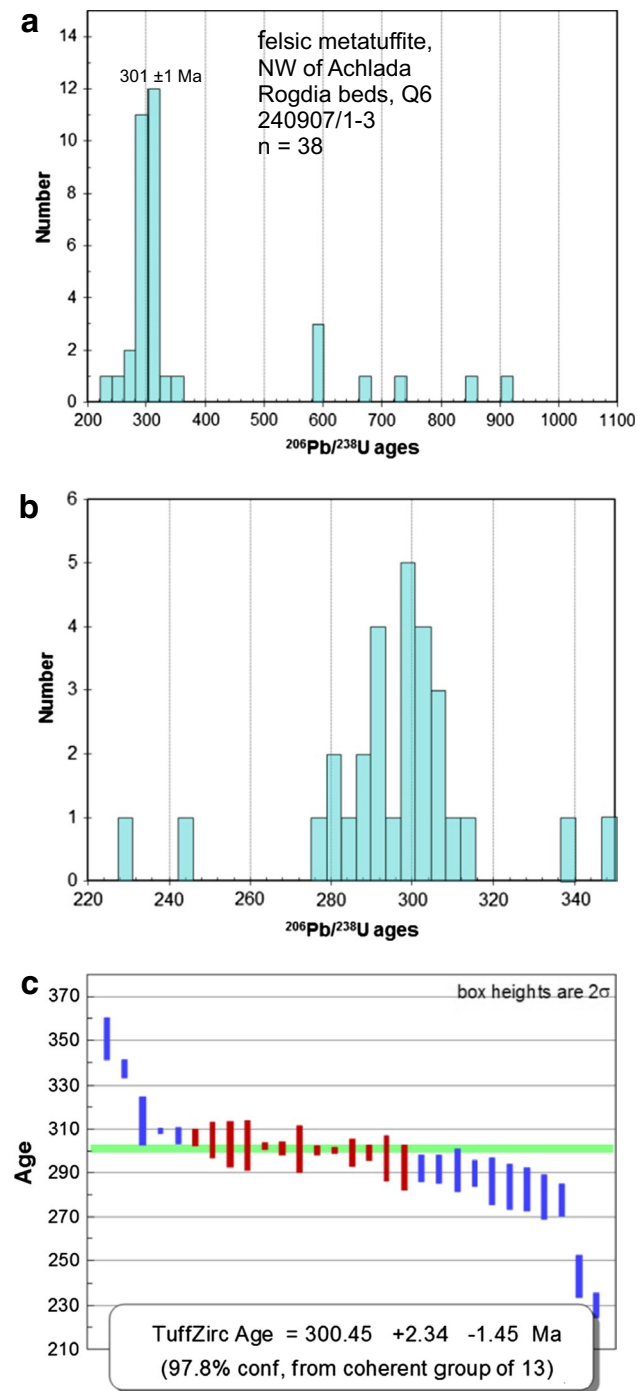
Fig. 13 Density plot of detrital zircons selected from felsic layer of the uppermost Rogdia Beds (Q6 subunit); sample 24-09-07/1-3

euhedral to subhedral in shape, whereas most of the Precambrian zircons are rounded (Fig. 14).

Vasilikon marble

All samples of Vasilikon marble were collected in its lower part close in contact to the Rogdia Beds. One of these *samples 031008/1-2* is located only few meters from the boundary to the Rogdia beds. It reflects the sheared contact along the road Sisses-Heraklion. This light marble shows a strong mylonitic foliation with a stretching lineation trending N–S. Calcite of this mylonitic sample has a maximum grain size of 0.8 mm. Most grains, however, are <0.1 mm in size. Large grains may result from previous veins, which are stretched in the N–S direction and show twins of type II and III (according to Burkhard 1993). Moreover, calcite is affected by pressure solution as is indicated by pressure solution seams and stylolites. There are discrete layers, which are rich in white mica, the latter up to 0.3 mm and oriented parallel to the mylonitic foliation. Detrital quartz grains are present, but only in few cases. Oblique fabrics in sections cut perpendicular to the mylonitic foliation and parallel to the lineation (*XZ*-sections) show SC fabrics and asymmetric orientation of white mica, which indicate a top-to-the-north sense of shear (Fig. 15a, b).

Sample 20050606-22 of reddish marble, exposed along a path cut between Fodele and Moni Savvathianon (N35°22′31″ E24° 59′ 20″, Fig. 2), shows foraminifera of the species *Meandrospira aff. pusilla* (Ho 1959) (Fig. 15c–f), which suggests a late Olenekian to early Anisian age for this part of the Vasilikon marble. Shallow water conditions during the deposition of the protolith of the Vasilikon marble are indicated by algae (Fig. 4e) in samples exposed ca. 1.5 km west of Achlada along the old road Achlada Fodele (sample 080915-1; E24°58′31″, N35°23′52″).

Achlada Beds

One felsic boulder of a strongly foliated metaconglomerate (*sample 080915/2*, Figs. 2, 4f) was collected from the basal part of the Achlada beds located 1 km north of Achlada along the old road Achlada–Fodele (E24°59′14,9″, N35°24′14,9″). Similar to the matrix of the metaconglomerate, the boulder itself shows a striking foliation, which is subparallel to the matrix foliation. The foliation results from the shape-preferred orientation of biotite and of plagioclase (Fig. 15g). Quartz is the most frequent mineral, which is largely recrystallized, particularly in the matrix of the boulder. The size of the matrix minerals is ca. 0.03 mm. Larger porphyroclasts show only undulatory extinction. Plagioclase is largely euhedral, up to 1 mm in size and is altered to albite. Deformation of plagioclase is indicated by fractures, deformation twins,

and Neoarchean (Fig. 13a). Two detrital zircons yielded subconcordant Triassic ages at 230 ± 6 and 244 ± 9 Ma. The major Carboniferous age peak is also supported by the ID-TIMS analyses, which yielded a concordia zircon age at 300.3 ± 0.9 Ma (Fig. 10c). It has to be emphasized that all of the younger zircons (Carboniferous to Triassic) are

Fig. 14 Representative cathodoluminescence (CL) images of analyzed zircons separated from the felsic layer of the uppermost Rogdia Beds (Q6 subunit); sample 24-09-07/1-3
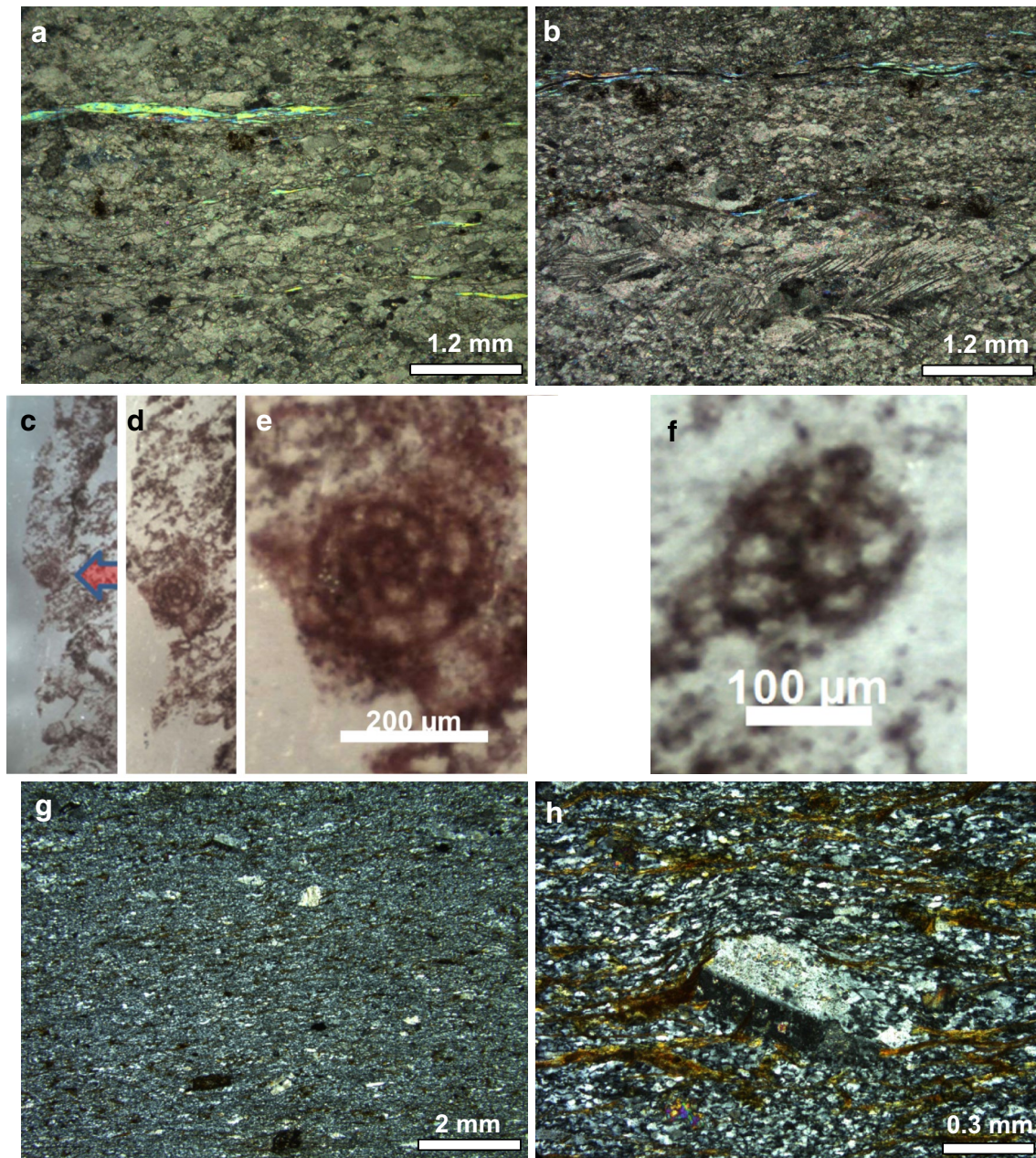
Fig. 15 Microphotographs showing deformation microfabrics and faunal content of Vasilikon and Achlada Beds. **a** Oblique alignment of white mica and elongated calcite grains, with respect to the main foliation (*horizontal* in the microphotograph), suggests top-to-the-north sense of shear in the Vasilikon marble close to the contact to the Rogdia Beds; sample 031008/1-2; crossed polarizers. **b** Oblique alignment of white mica and drag of twin lamellae in calcite, with respect to the main foliation (*horizontal* in the microphotograph), suggest top-to-the-north sense of shear in the Vasilikon marble; sample 031008/1-2; crossed polarizers. **c–f** Foraminifera *Meandrospira* aff. *pusilla* (Ho 1959) suggests a late Olenekian to middle Anisian age for a reddish layer intercalated inside Vasilikon marble; sample 20050606-22; parallel polarizers. **g** Overview of felsic (probably metarhyolite) pebble of foliated metaconglomerate of basal Achlada beds showing plagioclase and quartz porphyroclasts embedded in foliated and largely recrystallized matrix of quartz, plagioclase and biotite; sample 080915/2; crossed polarizers. **h** Close-up view of (**g**) showing altered plagioclase porphyroclast with asymmetric strain shadows of biotite; crossed polarizers

kink bands and boudinage. Many crystals show relics of a zonation with the central part being more strongly altered than the marginal part ('filled plagioclase'). Most plagioclase porphyroclasts show asymmetric pressure shadows consisting of fibrous quartz and phyllosilicate (Fig. 15h). The phyllosilicate phase is present in form of biotite, which sometimes has replaced plagioclase. There are few relics of hornblende or pyroxene, which are largely

replaced by biotite and epidote. Few large opaque phases show boudinage.

ID-TIMS dating of zircons separated from the felsic boulder described above yielded a concordant age at 242 ± 1.6 Ma (Supplementary Table 5; Fig. 10d), which is interpreted as the age of the protolith (probably a rhyolite). Together with the other analyzed zircons they define a discordia with intercepts at 0 +19/−19 and 246 +9/−8 Ma, respectively (Fig. 10d). When considering the uncertainty of the concordant zircon age, the (meta)conglomerate from which the felsic boulder was collected should have been deposited later than 244 Ma during the Anisian or later.

Discussion

Constraints on sedimentation ages

The youngest zircons of the *albite gneiss of the lower Rogdia Beds (Q2 subunit)* are Cambrian in age meaning that the deposition of the gneiss protolith must have occurred during the Cambrian or later. The Q2 subunit is underlain by the Maskali quartzite (Q1 subunit, Richter and Kopp 1983). A marble layer in Q1 subunit, exposed at Skilarmi hill, yielded a lower Triassic conodont fauna (Epting et al.

1972). However, it is not clear, if this marble layer is part of the Q1 subunit of the Rogdia Beds or is part of the Talea Ori (Plattenkalk) unit (König and Kuss 1980; Richter and Kopp 1983; Krahl et al. 1988). A Permian sedimentation age is possible, because the age spectrum of the detrital zircons, e.g., the Neoproterozoic cluster, is identical with a Permian sample of eastern Crete in the Phyllite–Quartzite Unit s.str. (Zulauf et al. 2014).

The youngest significant peak of detrital zircons collected from the *Q6 subunit of the Rogdia Beds (felsic metatuffite)* is present at ca. 290 Ma. For this reason, the deposition of the metatuffite and related clastic rocks (phyllite and quartzite) should have occurred in Sakmarian or younger times (Fig. 16). Apart from the early Permian and older detrital zircons, there are two younger zircons, which yielded subconcordant U–Pb ages at 244 ± 9 and 230 ± 6 Ma. Similar ages have been obtained from volcanics and from detrital zircons of the Tyros Unit of eastern Crete (249 ± 2, 242 ± 3, 240 ± 5, 237 ± 3, 228 ± 1 Ma; Zulauf et al. 2013, 2014). Moreover, the rhyolite boulder in the basal Achlada Beds also yielded a similar Triassic age (242 ± 2 Ma). Given the Triassic ages of the Q6 subunit are reliable, the deposition of this unit should have occurred in Ladinian or younger times. This age is in line with Scythian to Mid-Triassic fossils reported from the Rogdia Beds
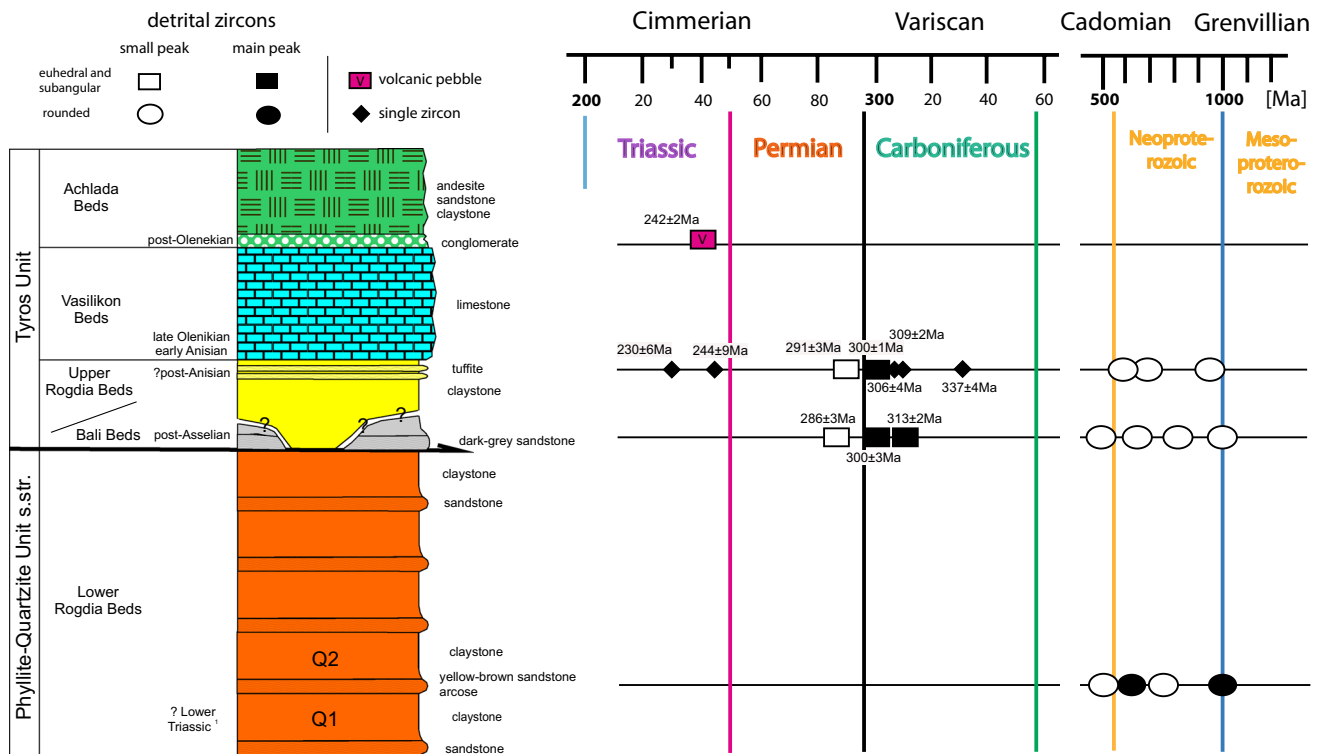

Fig. 16 Stratigraphic section of the studied rocks of the Talea Ori (without Alpine overprint) showing the distribution of U–Pb zircon ages obtained in the present study

(Krahl et al. 1988). A Ladinian or younger deposition of the uppermost Rogdia Beds is not consistent with the late Olenekian to early Anisian age that is indicated by the faunal content of the *Vasilikon marble*, which rests on top of the Rogdia Beds. However, if we assume few percent recent lead loss and taking into account only the older age with its uncertainty, the resulting age of 244–253 Ma (Inudsian to Olenekian) is in line with the age of the overlying *Vasilikon marble*. Further studies are necessary to solve this problem.

A maximum age for the deposition of the lowermost Achlada Beds is given by the concordant U–Pb zircon age of the rhyolite boulder (242 ± 2 Ma). Based on this age, the (meta)conglomerate from which this boulder has been collected should have been deposited in Anisian or younger times. This maximum age is compatible with the Olenekian to early Anisian age obtained for the deposition of the Vasilikon marble, which rests underneath the Achlada Beds.

Based on the youngest concordant zircons, the deposition of the dark gray metasandstone of Bali beach must have occurred after 289 Ma in Sakmarian or younger times. A similar conclusion has been drawn by Kock et al. (2007) based on Pb–Pb ages of detrital zircons obtained from a metasandstone collected further south (data on the exact locality have not been published). An early Permian maximum age for the deposition of the Bali metasandstone is in line with an Asselian age of the overlying dark metapelite of the Galinos Beds, based on fossils like brachiopods, trilobites, goniatites, bryozoans and crinoids (König and Kuss 1980; König 1982). However, it is not clear if the dark gray metasandstone analyzed by Kock et al. (2007) and in the present study is part of the Galinos Beds or belongs to the Rogdia Beds (Epting et al. 1972). Because of the striking similarity in the age spectra of detrital zircons of the Bali metasandstone and of the Q6 subunit of the uppermost Rodgia beds (Fig. 16), it is suggested that the Bali metasandstone does not belong to the Plattenkalk (Talea Ori) Unit, as suggested by Kock et al. (2007), but is forming the basal part of the upper Rogdia Beds.

Provenance of metasediments and their implication for paleogeography

The age spectrum of detrital zircons of the uppermost Rogdia beds with 57 % Upper Carboniferous zircons (Q6 subunit) is similar to that obtained from the lower part of the Tyros Unit (Chamezi: 66 % and Tripokefala Beds: 43 %, Permo-Triassic) and from the pre-Alpine basement (67 %) of eastern Crete. The detrital zircons of the felsic metatuffite of the uppermost Rogdia Beds show prominent peaks at 291 ± 3 and 301 ± 1 Ma (Figs. 13b, 16). Few concordant U–Pb zircons are present at ca. 306 ± 4, 309 ± 2 and 337 ± 4 Ma. Detrital zircons separated from pre-Alpine basement and from the lower Tyros Unit of eastern Crete

yielded similar concordia U–Pb ages at 290 ± 3 and 300 ± 2 Ma; zircons of magmatic boulders of conglomerates of the Tyros Unit yielded 291 ± 2 and 310 ± 4 Ma (Zulauf et al. 2014). There is also a striking similarity in the Triassic ages as has been shown in the previous section. For this reason, we correlate the uppermost part of the Rogdia Beds with the lower Tyros Unit of eastern Crete. This correlation is further justified by the fact that in both domains almost all zircons, which are younger than Silurian, are euhedral, meaning that the rocks from which these zircons are derived should have been exposed not far away from the basin in which the sediments and tuffites were deposited. Moreover, in both units the metasediments frequently include detrital quartz with perpendicular sets of subgrains, which indicate that the source rocks underwent high-grade metamorphism (deformation at T > ca. 650 °C; Passchier and Trouw 2005, and references therein).

Apart from the Carboniferous to Triassic detrital zircons, there is also a striking correlation when regarding the older zircons, although their amount is much lower. Zircon age peaks in the Ediacaran, Cryogenian and Tonian as well as the lack of Mesoproterozoic zircons, as observed in the Q6 subunit of the Rogdia Beds, is also characteristic for the zircons of the Tyros rocks of eastern Crete.

Based on the similarities mentioned above, we argue that the uppermost Rogdia Beds are forming a stratigraphic equivalent of the lower Tyros Unit of eastern Crete. Both units should have been deposited along the active convergent margin of southern Eurasia along which the Paleotethys was consumed by northward subduction (Stampfli et al. 2013; Zulauf et al. 2014).

A further rock that has been deposited at this site is the Bali metasandstone, detrital zircons of which yielded U–Pb age peaks at 286 ± 3, 288 ± 3, 300 ± 3, 302 ± 2, 310 ± 2 and 313 ± 2 Ma (concordia ages). Similar zircon ages had been obtained from Bali metasandstone using the Pb–Pb method (Kock et al. 2007). These Variscan-aged zircons of the Bali rocks are also largely euhedral (in contrast to the older zircons), and the detrital quartz grains also show evidence for high-grade metamorphism in the source domain. Moreover, the amount of ca. 45 % of Neoproterozoic zircons is similar to that obtained from eastern Crete (ca. 30 %), and there are also small Cambrian, Ediacaran, Cryogenian, Tonian and Stenian zircon age peaks in the Bali metasandstones, whereas Mesoproterozoic zircons are lacking. This Cambrian to Proterozoic age spectrum, and the Tonian/Stenian zircons in particular (up to 18 %), suggest that the source rocks of the Bali metasandstone are not derived from Variscan basement of central Europe (as suggested by Kock et al. 2007), but from the late Variscan orogeny situated at the southern active margin of Eurasia. Along this margin, the Paleotethys was consumed and Minoan-type terranes with an east Gondwanan
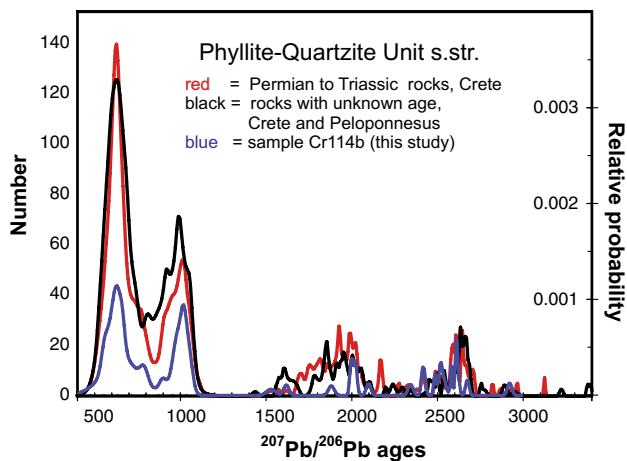
Fig. 17 Age spectra of detrital zircons separated from rocks of the Phyllite–Quartzite Unit s.str. of the External Hellenides (after Zulauf et al. 2014; Dörr et al. 2015; Chatzaras et al., this volume; and this study)

Fig. 18 Age spectra of detrital zircons separated from the Tyros and the Phyllite–Quartzite Unit s.str. of Crete (after Zulauf et al. 2014; Chatzaras et al., this volume; this study)

affinity collided with Eurasia (Zulauf et al. 2014). As dark gray metasandstone is lacking in the lower Tyros Unit of eastern Crete, but dark gray amphibolite facies quartzite, with a late Carboniferous/early Permian sedimentation age (302–283 Ma), is present in the Variscan basement underneath (Zulauf et al. 2014), it is possible that the dark gray Bali metasandstone is forming a stratigraphic equivalent of this basement quartzite or sandstone of the Chamezi beds (also only one peak at 310 Ma). This assumption is supported by the fact that 46 % of detrital zircons from the basement quartzite are Pennsylvanian with concordia ages at 321 ± 2, 310 ± 3, and 300 ± 3 Ma (Zulauf et al. 2014), which are almost identical to those of the Bali metasandstone.

Thus, the dark gray metasandstone of Bali does not belong to the Plattenkalk (Talea Ori) Unit (as has been proposed by Kock et al. 2007) but is part of the Tyros Unit.

The detrital zircon age spectrum of the Triassic albite gneiss of the lower Rogdia Beds (Q2 subunit) is entirely different compared to the age spectra of the rocks discussed above. Variscan-aged zircons are entirely lacking. The youngest zircons are Cambrian in age. These Cambrian zircons, together with similar amounts of Ediacaran, Cryogenian and Tonian zircons and the lack of Mesoproterozoic zircons suggests that the rocks of the Q2 subunit of the Rogdia Beds were deposited along the northern passive margin of east Gondwana. Similar detrital zircon age spectra have been obtained from the Triassic Phyllite–Quartzite Unit s.str. of eastern Crete (Dörr et al. 2015), and from the Phyllite–Quartzite Unit s.str. of western Crete and the Peloponnesus (Chatzaras et al. this volume) (Fig. 17).

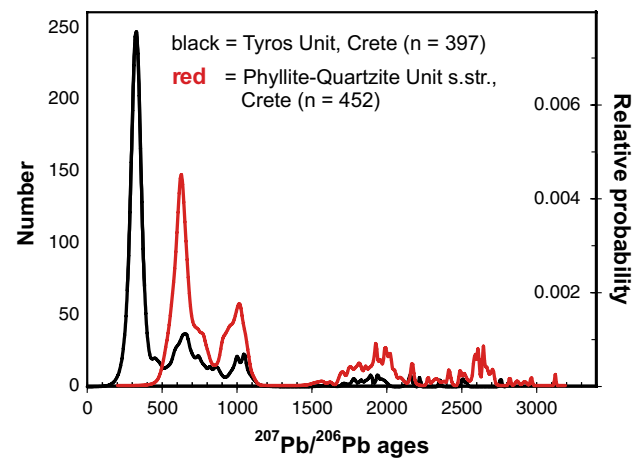The difference in detrital age spectra between the uppermost Rogdia Beds (including the Bali metasandstone) and the lower Rogdia beds (Fig. 16) suggests that the provenance areas of both are entirely different meaning that the Paleotethys suture should be situated inside the Rogdia Beds between the Q2 (northern margin of Gondwana or Cimmeria) and the Q6 (active southern margin of Laurasia) subunits. The striking difference between the detrital zircon age spectra of the Tyros and the Phyllite–Quartzite Unit s.str. is shown in Fig. 18. A local paleographical barrier can be excluded to explain the different detrital zircon age spectra, as the latter are widely distributed not only in the Hellenides, but also in Turkey (e.g., Abbo et al. 2015; Ustaömer et al. 2016). Moreover, Triassic rocks of the Tyros and of the Phyllite–Quartzite Unit s.str. show striking differences in sedimentary facies (e.g., Krahl et al. 1986; Robertson 2008, 2012), which is in line with a major suture zone. The possible trace of the Paleotethys suture in the External Hellenides is shown as orange broken line in Fig. 1 and is marked as a thrust nappe contact in Fig. 16.

The new Olenekian to early Anisian age of the Vasilikon marble suggests that the latter is a stratigraphic equivalent of the Chamezi marble of eastern Crete, which also yielded a lower Triassic age (Krahl et al. 1986). The Achlada Beds with Anisian or younger conglomerates at its base might form an equivalent of the Tripokefala Beds of eastern Crete, which are lower Anisian in age (Krahl et al. 1986).

Alpine structures and kinematics

All rocks investigated underwent Alpine subduction and related deformation under HP–LT metamorphic conditions (Theye and Seidel 1991). The dominant foliation with its N–S trending stretching/mineral lineation, described also by Chatzaras et al. (2006), does not result

from a first deformation event as proposed by Hall and Audley-Charles (1983) and by Richter and Kopp (1983), but from younger deformation (Chatzaras et al. 2006). In the studied rocks, relics of a first deformation event (D1) are preserved as internal fabric ($S_i = S_1$) inside albite blasts and as isoclinal intrafolial folds with respect to the dominant foliation (S_2). Such early internal fabrics ($S_i = S_1$) are also reported from chloritoid blasts (Chatzaras et al. 2006). In the study area, the early isoclinal folds affect blue amphibole (crossite; Seidel 1978), which should have grown during the prograde path of the HP–LT metamorphism. The axes of these early folds are sub-parallel to the N–S trending mineral/stretching lineation, which is a common phenomenon of the subducted rocks not only in the Talea Ori but all over Crete. In cases where these early folds are at a high angle to the N–S trending stretching lineation, they show a S vergence, and similar top-to-the-SSE sense of shear has also been described from asymmetric fabrics inside a mylonite at the contact between the Phyllite–Quartzite s.l. and the Plattenkalk Unit (Chatzaras et al. 2006).

The dominant foliation (S_2) of the studied rocks, however, results from top-to-the-north shearing at $T >$ ca. 400 °C as is indicated by recrystallized plagioclase and by the stability of biotite during these movements. Given the pre-D_2 blue amphiboles were aligned parallel to the D_2-stretching lineation, they underwent fracture boudinage during the shearing event. Top-to-the-north thrust movements have also been described by Richter and Kopp (1983). Elevated temperature during D_2 is also indicated by two sets of deformation twins in plagioclase. Type 2 twins in calcite, on the other hand, suggest $150 < T < 300$ °C (Burkhard 1993). However, these twins may have formed during the late stages of D_2, when the rocks were already exhumed to upper structural levels, meaning that D_2 was related to a retrograde metamorphic path and tectonic unroofing, which is typical for extensional movements. On the other hand, growth of biotite oblique to the S_2 fabric post-dates D_2 shearing.

Late north-vergent folding around E–W axes and related development of crenulation cleavage was active at higher structural levels and can be assigned as a D_3 event.

The early structures, with a top-to-the S kinematics should be related to the subduction event as has been described from the Phyllite–Quartzite Unit s.l. of eastern Crete (Zulauf et al. 2002). Moreover, also the top-to-the-north D_2 movements found in the Talea Ori rocks can be correlated with the top-to-the-north movements observed in eastern Crete as a third deformation event, that was also related to retrograde metamorphic conditions (D_3, Zulauf et al. 2002). Folding around E–W trending axes is also widespread in Crete where rocks of the Phyllite–Quartzite Unit s.l. are exposed.

Conclusions

The following conclusions can be drawn from the new data presented above.

- The striking difference in age spectra of detrital zircons inside different parts of the Rogdia Beds suggests that the Paleotethys suture should be situated between the lower Rogdia Beds, which belong to the Phyllite–Quartzite s.str. (northern passive margin of Gondwana), and the upper Rogdia Beds, which can be well correlated with the lower Tyros Beds of eastern Crete (southern active margin of Laurasia).
- The accurate location of the Paleothetys suture inside the Rogdia Beds has to be detected by further mapping combined with zircon age dating and microfabric analyses of detrital grains, such as quartz and feldspar.
- Similar different detrital zircon age spectra (late Paleozoic/Triassic vs. Precambrian) like those observed in the External Hellenides (Crete, Peloponnesus) are also present in Turkey, where the Karakaya complex of the Sakarya Zone and the Taurides could represent equivalents of the Tyros and the Phyllite–Quartzite s.str. Unit, respectively.
- The dark gray color of the Bali metasandstone combined with zircon age spectra, zircon shape and the type of detrital quartz grains suggest that the Bali rocks can be correlated with quartzites of the Variscan basement of eastern Crete. Further mapping, combined with microfabric, petrographic, and zircon, analyses are required to unravel the structural situation near Bali, which is still poorly constrained.
- The Vasilikon marble and the Achlada Beds of the Talea Ori are forming stratigraphic equivalents of the Chamezi marble and the Tripokefala Beds, respectively, both of which belong to the lower Tyros Unit of eastern Crete.
- Further investigations are required to prove if the contact between the uppermost Rogdia beds and the Vasilikon marble is a sedimentary contact, which was overprinted by Alpine shearing.

References

Abbo A, Avigad D, Gerdes A, Güngör T (2015) Cadomian basement and Paleozoic to Triassic siliciclastics of the Taurides (Karacahisar dome, south-central Turkey): paleogeographic constraints from U–Pb–Hf in zircons. Lithos 227:122–139

Bonneau M (1973) Sur les affinités ioniennes des „calcaires en plaquettes" épimétamorphiques de la Crète, le charriage de la série de Gavrovo-Tripolitza et la structure de l'arc egéen. Compte Rendus de l'Academie des Sciences Paris 277:2453–2456

Burkhard M (1993) Calcite twins, their geometry, appearance and significance as stress–strain markers and indicators of tectonic regime: a review. J Struct Geol 15:351–368

Cayeux L (1902) Sur la composition et l'age des terrains métamorphiques de la Crète. Compte Rendus de l'Academie des Sciences Paris 134:1116–1119

Chatzaras V, Xypolias P, Doutsos T (2006) Exhumation of high-pressure rocks under continuous compression: a working hypothesis for the southern Hellenides (central Crete, Greece). Geol Mag 143:859–876. doi:10.1017/S0016756806002585

Dercourt J, Ricou LE, Vrielynck B (eds) (1993) Atlas Tethys palaeoenvironmental maps. Gauthier-Villars, Paris

Dörr W, Zulauf G, Gerdes A, Lahayec Yann, Kowalczyk Gotthardt (2015) A hidden Tonian basement in the eastern Mediterranean: age constraints from U–Pb data of magmatic and detrital zircons of the External Hellenides (Crete and Peloponnesus). Precambrian Res 258:83–108

Epting M, Kudrass HR, Leppig U, Schäfer A (1972) Geologie der Talea Ori/Kreta. Neues Jahrb Geol Paläontol Abh 141:259–285

Franz L (1992) Die polymetamorphe Entwicklung des Altkristallins auf Kreta und im Dodekanes (Griechenland), Ferdinand Enke

Fytrolakis N (1967) Über einen Fossilfund im Metamorphikum von Ostkreta. Bull Geol Soc Greece 7:89–92

Fytrolakis N (1972) Die Einwirkung gewisser orogener Bewegungen und die Gipsbildung in Ostkreta (Prov. Sitia). Bull Geol Soc Greece 9(1):81–100

Hall R, Audley-Charles MG (1983) The structure and regional significance of the Talea Ori, Crete. J Struct Geol 5:167–179

Haude G (1989) Geologie der Phyllit-Einheit im Gebiet um Palekastro (Nordost-Kreta, Griechenland). PhD thesis, Technical University Munich, Germany

Ho Y (1959) Triassic foraminifera from the Chialingkiang Limestone of South Szechuan. Acta Paleontol Sin 7(5):387–418 **(in Chinese with English abstract)**

Jackson SE, Pearson NJ, Griffin WL, Belousova EA (2004) The application of laser ablation-inductively coupled plasma-mass spectrometry to in situ U–Pb zircon geochronology. Chem Geol 211:47–69

Katsiavrias N et al (2008) Geological map of Anoyia, Crete, 1:50000, 1st edn. Geological Survey of Greece, Athens

Kock S, Martini R, Reischmann T, Stampfli GM (2007) Detrital zircon and micropalaeontological ages as new constraints for the lowermost tectonic unit (Talea Ori unit) of Crete, Greece. Palaeogeogr Palaeoclimatol Palaeoecol 24:307–321

König H (1982) Unterpermische Seeigel aus Kreta (Griechenland). N Jahrb Geol Paläontol Mo 3:167–175

König H, Kuss SE (1980) Neue Daten zur Biostratigraphie des permotriadischen Autochthons der Insel Kreta (Griechenland). N Jahrb Geol Paläontol Monatsh 1980:525–540

Kozur H, Krahl J (1987) Erster Nachweis von Radiolarien im tethyalen Perm Europas. Neues Jahrbuch für Geologie und Paläontologie Monatshefte, Abhandlungen 174:357–372

Krahl J, Kaufmann G, Kozur H, Richter D, Förster O, Heinritzi F (1983) Neue Daten zur Biostratigraphie und zur tektonischen Lagerung der Phyllit-Gruppe und der Trypali-Gruppe auf der Insel Kreta (Griechenland). Geol Rundsch 72:1147–1166

Krahl J, Kauffmann G, Richter D, Kozur H, Möller I, Förster O, Heinritzi F, Dornsiepen U (1986) Neue Fossilfunde in der Phyllit-Gruppe Ostkretas (Griechenland). Z Dt Geol Ges 137:523–536

Krahl J, Richter D, Förster O, Kozur H, Hall R (1988) Zur Stellung der Talea Ori im Bau des kretischen Deckenstapels (Griechenland). Z Dtsch Geol Ges 139:191–227

Ludwig KR (2001) Isoplot/Ex—a geochronological toolkit for Microsoft Excel. Berkley Geochronology Center Special Publication 1a

Nasdala L, Hofmeister W, Norberg N, Mattinson JM, Corfu F, Dörr W et al (2008) Zircon M257—a homogeneous natural reference material for the ion microprobe U–Pb analysis of zircon. Geostand Geoanal Res 32:247–265

Passchier CW, Trouw RAJ (2005) Microtectonics. Springer, Berlin

Richter D, Kopp KO (1983) Zur Tektonik der untersten geologischen Stockwerke auf Kreta. N Jb Geol Paläont Monatsh 1983:27–46

Robertson AHF (2006) Sedimentary evidence from the south Mediterranean region (Sicily, Crete, Peloponnese, Evia) used to test alternative models for the regional tectonic setting of Tethys during Late Palaeozoic-Early Mesozoic time. In: Robertson AHF, Mountrakis D (eds) Tectonic development of the Eastern Mediterranean region, vol 260. Geological Society of London, Special Publications, pp 91–154

Robertson AHF (2008) Late Palaeozoic–Early Mesozoic metasedimentary and metavolcanic rocks of the Phyllite–Quartzite Unit, eastern Crete (Greece): an extensional, rift-related setting for the southern margin of Tethys in the Eastern Mediterranean region. Z Dtsch Ges Geowiss 159:351–374

Robertson AHF (2012) Late Palaeozoic–Cenozoic tectonic development of Greece and Albania in the context of alternative reconstructions of Tethys in the Eastern Mediterranean region. Int Geol Rev 54:373–454

Romano SS, Dörr W, Zulauf G (2004) Cambrian granitoids in pre-Alpine basement of Crete (Greece): evidence from U-Pb dating of zircon. Int J Earth Sci 93:844–859

Romano SS, Brix MR, Dörr W, Fiala J, Krenn E, Zulauf G (2006) The Carboniferous to Jurassic evolution of the pre-Alpine basement of Crete: constraints from radiometric dating of orthogneiss, fission-track dating of zircon and structural/petrological data. In: Robertson AHF, Mountrakis D (eds) Tectonic development of the Eastern Mediterranean region, vol 260. Geological Society London, Special Publications, pp 69–90

Sannemann W, Seidel E (1976) Die Triasschichten von Rawdoucha/NW-Kreta. Ihre Stellung im kretischen Deckenbau. Neues Jahrbuch für Geologie und Paläontologie Monatshefte 1976:221–228

Seidel E (1978) Zur Petrologie der Phyllit-Quarzit-Serie Kretas. Habilitationsschrift, Universität Braunschweig, p 1–145

Seidel E, Kreuzer H, Wilhelm H (1982) A late Oligocene/early Micocene high pressure belt in the external Hellenides. Geol Jahrb E32:165–206

Stacey JS, Kramers JD (1975) Approximation of terrestrial lead isotope evolution by a two-stage model. Earth Planet Sci Lett 26:207–221

Stampfli GM, Hochard C, Vérard C, Wilhelm C, von Raumer J (2013) The formation of Pangea. Tectonophysics 593:1–19

Theye T, Seidel E (1991) Petrology of low-grade high-pressure metapelites from the External Hellenides (Crete, Peloponnese). A case study with attention to sodic minerals. Eur J Mineral 3:343–366

Ustaömer T, Ustaömer PA, Robertson AHF, Gerdes G (2016) Implications of U–Pb and Lu–Hf isotopic analysis of detrital zircons for the depositional age, provenance and tectonic setting of the Permian–Triassic Palaeotethyan Karakaya Complex, NW Turkey. Int J Earth Sci 105:7–38. doi:10.1007/s00531-015-1225-8

Xypolias P, Doutsos T (2000) Kinematics of rock flow in a crustal-scale shear zone: implication for the orogenic evolution of the southwestern Hellenides. Geol Mag 137:81–96

Xypolias P, Chatzaras V, Koukouvelas I (2007) Strain gradients in zones of ductile thrusting: insights from the External Hellenides. J Struct Geol 29:1522–1537

Zulauf G, Kowalczyk G, Krahl J, Petschick R, Schwanz S (2002) The tectonometamorphic evolution of high-pressure low-temperature

metamorphic rocks of eastern Crete, Greece: constraints from microfabrics, strain, illite crystallinity and paleostress. J Struct Geol 24:1805–1828

Zulauf G, Blau J, Dörr W, Klein T, Krahl J, Kustatscher E, Petschick R, van de Schootbrugge B (2013) New U–Pb zircon and biostratigraphic data of the Tyros Unit, eastern Crete: constraints on Triassic palaeogeography and depositional environment of the eastern Mediterranean. Z Dtsch Ges Geowiss 164:337–352

Zulauf G, Dörr W, Fisher-Spurlock SC, Gerdes A, Chatzaras V, Xypolias P (2014) Closure of the Paleotethys in the External Hellenides: constraints from U–Pb ages of magmatic and detrital zircons (Crete). Gondwana Res. doi:10.1016/j.gr.2014.06.011